An evaluation of spatial correlation functions in textural analysis of metamorphic rocks

David M. Hirsch[1], Richard A. Ketcham[2] and William D. Carlson[3]

Department of Geological Sciences, The University of Texas at Austin, Austin, Texas, 78712, USA, [1]<dhirsch@mail.utexas.edu>, [2]<richk@maestro.geo.utexas.edu>, [3]<wcarlson@mail.utexas.edu>
(Received January 13, 2000; Published June 2, 2000)

Abstract

Spatial correlation functions, which quantify spatial relationships among porphyroblasts over a range of length scales, can be used in combination with other techniques of quantitative textural analysis to constrain crystallization mechanisms in metamorphic rocks. The utility, reliability, and robustness of these functions, however, depend critically upon correct methods of calculation and application to geological samples.

Application of the L'-function, Pair Correlation Function, and Mark Correlation Function (Stoyan and Stoyan, 1994) to artificial arrangements of crystals yields results consistent with their predetermined ordering and clustering qualities. These results serve as a foundation for the interpretation of more complex simulated and natural crystal arrays. Analysis of artificial and simulated crystal arrays in which ordering signals are obscured in various ways (displacing crystals in an ordered array by increasing amounts, reducing the number of crystals, and increasing the sample's aspect ratio) demonstrates that these scale-dependent functions are robust indicators of effects diagnostic of certain crystallization mechanisms, even in complex circumstances. The effects of clustering of nucleation sites, however, can strongly obscure any underlying signal that might reveal crystallization mechanisms.

The L'-function and the Pair Correlation Function are sensitive to short-range ordering of crystals, which may reflect suppression of nucleation in the vicinity of growing porphyroblasts. The Mark Correlation Function is sensitive to size-isolation correlations, which may reflect retardation of growth among crystals competing for nutrients. Interpretation of these functions, however, requires careful attention to proper calculation of Monte Carlo simulations, which are used to identify values of the functions that constitute a null-hypothesis region for comparison to samples with unknown ordering and clustering characteristics. To yield functional values commensurate with those calculated for a particular natural rock specimen, each simulation must match as closely as possible several critical features of the natural rock, including the set of crystal radii, limitations on the observability of crystals, and the shape and size of the bounding surface of the sample.

Crystallization mechanisms in seven previously studied garnetiferous rocks from three localities (Carlson *et al.*, 1995; Denison and Carlson, 1997) have been re-assessed using both scale-dependent correlation functions and single-valued spatial statistics, both evaluated by

comparison to rigorously computed null-hypothesis regions. The results confirm previous inferences that the nucleation and growth rates of the garnet porphyroblasts in these specimens were governed by rates of diffusion through the intergranular medium.

Keywords: Quantitative textural analysis, garnet, porphyroblast, correlation functions

Introduction

Porphyroblast crystallization in metamorphic rocks results from the interplay of several atomic-scale processes involved in nucleation and growth. Because these cannot be directly observed, we must infer their relative importance and rates by reference to features in natural samples. One such avenue to understanding the kinetics of porphyroblast crystallization is through quantitative analysis of metamorphic textures. An obvious requirement for this is the existence of textural measures that discriminate among various processes that may have operated in the rocks during metamorphic recrystallization.

Recently, spatial correlation functions taken from the statistics literature and in use in the biological sciences have been proposed as promising tools for textural analysis (Raeburn, 1996; Daniel and Spear, 1999). This study examines these statistical measures to determine their utility, reliability, and extent of agreement with previously used statistics and other tools used to infer details of metamorphic processes and their kinetics.

Background: diffusional vs. interfacial controls on nucleation and growth

During the crystallization of a metamorphic mineral, a number of interconnected processes must occur, as documented by numerous workers (Carmichael, 1969; Spry, 1969; Kretz, 1973, 1974; Walther and Wood, 1984; Rubie and Thompson, 1985; Ridley and Thompson, 1986; Carlson, 1989; Joesten, 1991; Kerrick *et al.*, 1991; Kretz, 1994; Rubie, 1998). There must be heat input for the reaction to progress, if it is endothermic; the reactants must dissolve into the intergranular medium; chemical components of the mineral must diffuse through or be transported by the medium to the surface of the growing crystal; they must be incorporated into the structure of the crystal; and chemical species produced by the reaction but not incorporated into the crystal must diffuse or be transported away from the growing porphyroblast. Whichever of these sequential processes is the slowest will determine the overall rate of the reaction (Fisher, 1978). Because heat-flow control implies extremely limited nucleation, it is not thought to be a rate-limiting process during most episodes of metamorphic crystallization. The goal therefore reduces to discerning the differing effects of diffusional versus interfacial control on nucleation and growth. As described in Kretz (1974) and Carlson (1989), diffusional control (slow intergranular diffusion relative to the rate of surface reactions) affects both nucleation and growth. As preexisting crystals reduce the chemical affinity for reaction in their neighborhood by depleting the local nutrient supply, nucleation in this nearby region is suppressed, which leads to spatial ordering of crystal centers relative to an interface-controlled case (Fig. 1). Continued reduction in chemical affinity near growing crystals causes the depleted zones for adjacent crystals to impinge, so these crystals tend to be smaller than more isolated crystals that nucleated at the same time (Fig. 2).

These effects of diffusional control on crystallization have measurable macroscopic consequences: the resulting textures should tend towards spatial ordering and should embody correlations between a crystal's size and measures of its degree of isolation. Spatial correlation functions can reveal these effects, and thus provide tests of competing hypotheses for the mechanisms that govern the crystallization of porphyroblasts.

In our description of the presumed effects of diffusion control on metamorphic textures, it is implicitly assumed that the precursor is sufficiently fine-grained so as to be uniform at the scale of a porphyroblast's depleted zone. This is required because heterogeneous nucleation on preferred surfaces of certain phases could control the distribution of nucleation sites, and the distribution of precursor phases that supply the reactant species can control the rate and amount of growth. To the extent that favored nucleation sites and localized sources of nutrients are inhomogeneously distributed at the scale of observation, textural features will depart from the idealized cases described below. As described below, part of the utility of correlation functions lies in their ability to identify such departures.

Correlation functions

Previous work

A number of statistics have been used previously to quantify the ordering effects induced by diffusional control on nucleation and growth, and thereby distinguish between diffusional and interfacial control on nucleation and growth of porphyroblasts. These include the ordering index, the clustering index, and the impingement index (Kretz, 1974; Carlson, 1989; Denison *et al.*, 1997). Recently, a new class of statistics has been proposed as improvements on these previously used measures of ordering and clustering (Raeburn, 1996; Daniel and Spear, 1999). These correlation functions, which measure the number or sizes of crystals whose centers are separated by a given distance, have the advantage of measuring a given statistic over a range of length scales, in contrast to single-valued statistics, which do not have this type of scale dependency.

The three correlation functions examined here are the *L*-function, the Pair Correlation Function, and the Mark Correlation Function. Ripley (1976) first introduced a *K*-function, which, when normalized, gives his *L*-function. Other workers have developed derivatives of the *K*-function, which are briefly reviewed in Konig (1991). Those used in this work are the *L*-function, the Pair Correlation Function and the Mark Correlation Function. Each of these functions as used for this work is described in detail below.

Correlation functions were first employed in the spatial statistics literature to describe ordering and clustering of point arrays, and have since been applied principally in the biological and physical sciences. They were used for textural analysis of crystals in metamorphic rocks first by Raeburn (1996), then by Daniel and Spear (1999). These studies inferred interfacial controls on crystallization, in contrast to prior work using other statistical methods that inferred diffusional controls on nucleation and growth in a variety of samples (Carlson, 1989, 1991; Carlson and Denison, 1992; Denison and Carlson, 1997; Denison *et al.*, 1997). The contrast between these results raised the possibility that different statistical approaches might be responsible for differences in inferred mechanisms, although Hirsch and Carlson (1997) used

correlation functions to confirm earlier inferences of diffusional control based on single-valued statistics.

It is important to note that statistical measures are not the only method of distinguishing diffusional controls from interfacial controls. Another approach is that of iterated domain calculations (Denison *et al.*, 1997). In this method, diffusional control is assumed, and each crystal is assigned a nucleation time based upon its size. Nucleation and growth of the natural crystal array is simulated, and inconsistencies between the simulation and the natural rock are progressively removed through iteration by adjusting the nucleation times assigned to each crystal. Samples that do not converge towards a solution, or that lead to physically impossible geometries, are deemed to violate the initial assumption of diffusion control. Also, chemical means of discrimination in the form of Kretz's (1974) normalized radius-rate diagrams have also been widely used for zoned garnet (Kretz, 1974; Carlson, 1989; Raeburn, 1996; Denison and Carlson, 1997; Daniel and Spear, 1999). These alternative approaches should be used whenever possible to provide independent tests of conclusions drawn from spatial statistics.

The L' -function

The L' -function is a slightly modified version of the L-function, the value of which is related to the number of crystal centers within a certain distance of each crystal center. The L' -function is positive if there are more crystal centers within this distance than would be expected if the crystal centers were Poisson-distributed (spatially random and sparse), and negative if there are fewer. A schematic illustration useful for understanding these functions appears in Figure 3.

The basis for the calculation is the K-function (Ripley, 1976), which measures the number of crystal centers within a certain distance r of each crystal center (Fig. 3). The K-function, $K(r)$, can be estimated using the quantity $\hat{k}_2(r)$, an unbiased estimator for $\lambda^2 K(r)$, where λ in this discussion is the number of crystals per unit volume (Stoyan and Stoyan, 1994, p. 280). The estimator $\hat{k}_2(r)$ is calculated from

$$\hat{k}_2(r) = \sum_{i=1}^{n} \sum_{\substack{j=1 \\ (j \neq i)}}^{n} \frac{I\left(r, \left\| \bar{x}_i - \bar{x}_j \right\|\right)}{V(W)}, \tag{1}$$

where n is the number of crystals in the sample region W, $\bar{x}_i$ is the vector from an arbitrary but consistent origin to the center of crystal i, $V(W)$ is the volume of the sample region, r is a specified test distance, $\|\bar{x}_i - \bar{x}_j\|$ is merely the distance between crystals i and j, which we can denote d, and $I(r,d)$ is an indicator function that takes the value zero if $d > r$, and the value unity if $d \leq r$. In this and the following presentation of the mathematical basis for the correlation functions, symbols conform to the usage of Stoyan and Stoyan (1994).

The K-function has a value of $(4/3)\pi r^3$ for a homogeneous randomly distributed array of crystal centers, a greater value at a given test distance for clustered arrays, and a smaller value for ordered arrays. The reason for this becomes clear when one considers that for a Poisson distribution,

$$\hat{k}_2(r) \approx \frac{n_{total}n_{d\leq r}}{V(W)}, \qquad (2)$$

and so the *K*-function tends towards

$$K(r) = \frac{\hat{k}_2(r)}{\lambda^2} \approx \left(\frac{n_{total}n_{d\leq r}}{V(W)}\right)\left(\frac{V(W)}{n_{total}}\right)\left(\frac{V_{d\leq r}}{n_{d\leq r}}\right) = V_{d\leq r} = \frac{4\pi r^3}{3}, \qquad (3)$$

where $n_{d\leq r}$ is the number of crystals within a spherical examination region of radius *r* and $V_{d\leq r}$ is the volume of this spherical region. The approximation is present because we are treating the number of crystals per unit volume, λ, first as $n_{total}/V(W)$ and then as $n_{d\leq r}/V_{d\leq r}$. An equality would imply that the number of crystals per unit volume in any spherical sub-region of radius *r* is identical to the bulk crystal number density, while in real rocks that grow from a uniform precursor, these values are close but not identical. The *K*-function is somewhat unwieldy, so most workers, beginning with Ripley (1976), have used a normalized version, the *L*-function. For analysis in three dimensions, the *L*-function is related to the *K*-function by

$$L(r) = \sqrt[3]{\frac{3K(r)}{4\pi}}, \qquad (4)$$

making the value of the *L*-function simply *r* for Poisson-distributed (spatially random) arrays. In the present work, there is a further normalization, here denoted *L'* (this normalization was included in the definition of *L(r)* given in Cressie, 1993),

$$L'(r) = L(r) - r, \qquad (5)$$

performed so that the value of the function will be zero for a Poisson-distributed array.

For crystals that nucleated and grew by an interface-controlled mechanism, one would expect only a small degree of ordering at the smallest length scales, due solely to the "volume effect," the inability to nucleate a new crystal inside the volume of a pre-existing crystal. The volume effect would be expected to cause ordering on scales only up to approximately the mean crystal diameter. For crystals that nucleated and grew under diffusional controls, one would expect significant ordering (negative values of *L'*) at scales over which diffusion was operating, typically up to about half the mean nearest-neighbor distance. Clustering of crystal centers, if present, should be reflected as positive values of the *L'*-function at the scale of the clustering.

The Pair Correlation Function

The Pair Correlation Function (PCF) is related to the *L'*, *L*, and *K*-functions; it also measures the number of crystal centers relative to each crystal center. However, instead of counting centers that lie *within* a certain distance of each crystal, the PCF identifies centers that lie *at or near* a certain distance from each crystal. The mathematical selection of crystals that satisfy this criterion is performed using a kernel function, the bandwidth of which dictates the amount by which the separation of two crystals may differ from the test distance and still allow those crystals to be included in the calculation (Fig. 4). The summation is normalized by an appropriate factor such that the PCF will yield a value of unity for a Poisson-distributed array.

The Pair Correlation Function, $g(r)$, is related to the "product density function", $\rho^{(2)}(r)$, by

$$g(r) = \frac{\rho^{(2)}(r)}{\lambda^2} \quad (r \geq 0). \tag{6}$$

Note that the "2" in $\rho^{(2)}(r)$ is not a power, but signifies the second-order product density. The product density function is essentially the probability that two crystal centers are separated by a distance r. In calculating the PCF, the product density function, $\rho^{(2)}(r)$, is first estimated by the quantity $\hat{\rho}(r)$ and this value is divided by the square of the crystal number density, estimated using

$$\hat{\lambda}^2 = \frac{n(n-1)}{[V(W)]^2}, \tag{7}$$

where n is the number of crystal centers in the sample. This estimator is used in favor of $[n/V(W)]^2$ because this alternative is biased, while equation (7) is unbiased (Ripley, 1981, p. 159). The estimator $\hat{\rho}(r)$ is calculated as

$$\hat{\rho}(r) = \sum_{i=1}^{n} \sum_{\substack{j=1 \\ (j \neq i)}}^{n} \frac{e_h\left(r - \left\| \vec{x}_i - \vec{x}_j \right\| \right)}{4\pi r^2}, \tag{8}$$

in which $e_h(t)$ is the Epanecnikov kernel function of bandwidth h, calculated as

$$e_h(t) = \begin{cases} \dfrac{3}{4h}\left(1 - \dfrac{t^2}{h^2}\right) & |t| \leq h \\ \\ 0 & \text{otherwise} \end{cases}, \tag{9}$$

where t is the value of the function to which the kernel is being applied, and h is the bandwidth of the kernel function.

The Epanecnikov kernel function serves both to limit the calculation to those crystals present in a spherical shell around crystal i, and to allow smoothing of the function by including larger numbers of crystals in each calculation. Crystals whose centers lie near the middle of the two-bandwidth shell (*i.e.*, close to the actual test distance) are weighted more heavily than those near the edge of the shell. In the present work, increments of r are chosen so that the shells are overlapped by 50%, or one bandwidth, to allow all crystals to fall within the heavily-weighted region of the calculation for some value of r. Stoyan and Stoyan (1994, p. 285) suggest that the value h for the bandwidth of the kernel function should be $h = c\,\lambda^{-1/2}$, with c in the range 0.1 - 0.2. In the present work, the value for c has been set to 0.1, out of a desire for detail in the statistics. Larger values of c (and therefore, h) will produce smoother curves; smaller values will produce more irregular curves, because fewer crystals, over a smaller range of test distances, will be used in the calculation (Fig. 5).

For an interface-controlled case, one expects a small degree of ordering (PCF < 1) at scales on the order of the mean crystal diameter, due to the volume effect. For a diffusion-controlled case, one expects a significant degree of ordering at the scales over which nucleation is suppressed, roughly half the mean nearest-neighbor distance.

The L'-function and the PCF measure similar aspects of the data, but are differentially sensitive to certain elements of the data. The L'-function counts crystals within a solid sphere centered at each crystal, while the PCF counts those within a spherical shell of fixed thickness (twice the kernel bandwidth h). The L'-function is more sensitive to clustering effects in the data, because when examining a crystal near the center of a spherical cluster with a test distance near the cluster radius, the L'-function will count all crystals within the cluster; the PCF will only count those crystals on the edge. This disparity will be increased if the crystal under consideration is offset by at least h from the cluster center, because the L'-function will still count most of the crystals in the cluster, while the PCF will now have half or more of its shell outside the cluster boundary. This effect will be maximized for spherical clusters, but should still apply for layered crystal arrays.

The Mark Correlation Function

The Mark Correlation Function (MCF) is closely related to the PCF, in that it similarly evaluates crystals within a certain bandwidth at a certain distance, but it weights its evaluation by some feature of the crystals, such as radius or volume. The MCF was calculated on selected samples first with crystal radius and then with crystal volume as the mark, and the difference in the MCF was found to be minor. Radius was chosen as the mark for consistency with previous work. Thus, as applied here, the MCF is a measure of the radii of crystals at a given separation. It will be less than unity if the radii of crystals separated by r have a geometric mean smaller than the mean radius of all the crystals in the sample.

It is worth noting one might choose two possible volumes (and therefore, radii) for a crystal that interpenetrates with another. One might imagine a plane separating the two crystals and assign the volume on each side of the plane to each crystal; alternatively, one might fit the best crystal shape (for garnets, we approximate this as a sphere) to each crystal and assign each the corresponding volume. By analogy to the terminology of Avrami (1940), we term the former the "actual volume" and we term the latter the "extended volume" (Carlson, 1989) as it will always be larger than the actual volume. The extended volume represents the size each crystal would have if growing in isolation, discounting diffusional growth-suppression effects. This choice of volumes will also affect the crystal center that is assigned, because that is calculated as the center of mass of the crystal. In the present work, we have chosen always to use the extended volume, as the crystal centers thus identified more closely correspond to the presumed nucleation location. Additionally, as the extended volume is independent of overlap, the crystal size distributions do not change upon rearrangement of locations in the production of null-hypothesis simulations, described below.

Other recent workers in the field have termed the Mark Correlation Function described here, or variations on it, the Mark Covariance Function, terminology that stems from Konig *et al*.

(1991). This paper adheres instead to the terminology of Stoyan and Stoyan (1994), who denote the Mark Correlation Function as $k_f(r)$ and define its estimator as:

$$\hat{k}_f(r) = \frac{\kappa_{mm}(r)}{\kappa_{mm}(\infty)}, \quad r \geq 0, \tag{10}$$

where $\kappa_{mm}(r)$ is estimated by

$$\hat{\kappa}_{mm}(r) = \frac{\hat{\rho}_{mm}(r)}{\hat{\rho}(r)}. \tag{11}$$

In this equation, $\hat{\rho}_{mm}(r)$ is an estimator for the mark product density function and $\hat{\rho}(r)$ is the estimator given above for the product density function. Their ratio can be interpreted as the conditional mean of $m_i m_j$, given that there are two points separated by a distance r (Stoyan and Stoyan, 1994, p. 263). Here, m_i is the radius of the ith crystal. Note that in order to preserve consistency with the definition given by Stoyan and Stoyan (1994), r in equations (10) and (11) represents not the radius of a crystal, but the test distance. Also, in equation (10) the subscript "f" indicates a generalized mark function. In this discussion we use two mark functions: $f=mm$ indicates the product of the marks (which is then normalized to give the geometric mean of the marks); $f=\overline{m}$ indicates the arithmetic mean of the marks. The mark product density function is calculated in a manner similar to the product density function:

$$\hat{\rho}_{mm}(r) = \sum_{\substack{i=1 \\ }}^{n} \sum_{\substack{j=1 \\ (j \neq i)}}^{n} \frac{m_i m_j e_h \left(r - \left\| \vec{x}_i - \vec{x}_j \right\| \right)}{4 \pi r^2}, \tag{12}$$

where m_i is the radius of the ith crystal. Stoyan and Stoyan (1994) also state that

$$\kappa_{mm}(\infty) = \overline{m}^2 \tag{13}$$

where $\overline{m}$ is the arithmetic mean radius of all the crystals in the sample.

Because $\hat{\rho}(r)$ and $\hat{\rho}_{mm}(r)$ contain many of the same normalization factors, and the same kernel function, the MCF estimator reduces to:

$$\hat{k}_{mm}(r) = \frac{1}{n(n-1)} \sum_{\substack{i=1 \\ }}^{n} \sum_{\substack{j=1 \\ (j \neq i)}}^{n} \left[\frac{m_i m_j}{\overline{m}^2} \cdot I\left(h, \text{Abs}\left(r - \left\| \vec{x}_i - \vec{x}_j \right\| \right) \right) \right], \tag{14}$$

where the second factor inside the brackets is the same indicator function as in Equation (1), which serves simply to exclude crystals whose centers do not lie inside the bandwidth region.

The MCF does not measure departures from spatially random distributions of crystal centers (ordering and clustering) as do the L'-function and the PCF; instead it is sensitive to localized variations in crystal size, and thus relative growth. For an interface-controlled case, one expects at the smallest scales to have a slight reduction in the MCF value (MCF < 1) by virtue of the fact

that at a given test distance r, it is unlikely to have a crystal in the calculation whose radius is greater than r, for that would require one crystal to be located inside another. (Specific criteria for the maximum overlap of crystals in an interface-controlled sample are discussed below.) For the diffusion-controlled case, however, one would expect significant suppression of growth for closely spaced crystals due to competition for nutrients, giving a value for the MCF significantly below unity at those scales over which diffusion is retarding growth, again roughly half the mean nearest-neighbor distance.

The MCF as described above has a small inherent bias towards values less than unity, because for each summand it in effect compares the pairwise geometric mean radius $[(m_i m_j)^{1/2}]$ to the arithmetic mean radius $[0.5*(m_i + m_j)]$ for the sample. The geometric mean for a set of positive numbers is always less than or equal to the arithmetic mean, so in the average, the summands for the MCF will be smaller than unity. This can be illustrated with a rock made up of three crystals, whose radii are 3, 10, and 50 units. If the MCF shown above is calculated using all the crystals in any rock (i.e., they are all separated by the test distance r), the expected unbiased value is unity. However, doing the actual calculation, we find that:

$$\hat{k}_{mm}(r) = 3^{-1}2^{-1}441^{-1}(30 + 150 + 30 + 500 + 150 + 500) = 0.514. \tag{15}$$

This bias toward values less than unity is magnified with small numbers of crystals that have a large variance (as in this example); in less extreme cases, it will not strongly skew the results. However, in light of this bias, the following variant of the Mark Correlation Function is proposed, in which the arithmetic mean of each pair of crystals is substituted for the geometric mean:

$$\hat{k}_{\overline{m}}(r) = \frac{1}{n(n-1)} \sum_{i=1}^{n} \sum_{\substack{j=1 \\ (j \neq i)}}^{n} \left[\frac{m_i + m_j}{2\overline{m}} \cdot I\left(h, \mathrm{Abs}\left(r - \left\| \overline{x}_i - \overline{x}_j \right\| \right)\right) \right] \tag{16}$$

For the above example, this gives:

$$\hat{k}_{\overline{m}}(r) = 3^{-1}2^{-1}42^{-1}(13+53+13+60+53+60) = 1.0. \tag{17}$$

In tests that we have performed, this proposed variant of the MCF shows the same qualitative patterns as $k_{mm}(r)$, and gives the expected results on simulations. Previous workers were led to prefer the geometric mean because the bias is small for most sets of data, and excursions from Poisson distributions are more easily recognized using the geometric mean. The proposed variant is therefore a more conservative approach, less prone to provide spurious indications of growth suppression. Throughout this article, we employ this variant based on the arithmetic mean.

Consistency with previous work

Raeburn (1996) and Daniel and Spear (1999) use somewhat different definitions for these correlation functions, drawn from Konig (1991). In the present work, we have carefully followed the nomenclature and definitions given in Stoyan and Stoyan (1994). Some differences are

merely semantic (e.g., others have used the term "Mark Covariance Function," which is not found in Stoyan and Stoyan, 1994), but there is one substantive difference in the function definitions, which will affect the value obtained from the Pair Correlation Function.

In Raeburn (1996) and Daniel and Spear (1999), the Konig (1991) definition for the PCF is given:

$$\rho^{(2)} = \sum_{i=1}^{n} \sum_{\substack{j=1 \\ j \neq i}}^{n} \frac{\mathbf{k}_h\left(r - \left\|p_i - p_j\right\|\right)}{4\pi\left(\left\|p_i - p_j\right\|\right)^2 \cdot \text{Vol}\left\{W_{p_i} \cap W_{p_j}\right\}}. \tag{18}$$

In this equation, $\mathbf{k}_h(r)$ is the Epanecnikov kernel function of bandwidth h (denoted as $\mathbf{e}_h(r)$ in the present work), the Vol{} term represents the translation edge-correction method detailed below, r is the test distance, and $\|p_i - p_j\|$ is the distance between crystals i and j. This is in contrast with the definition from Stoyan and Stoyan (1994) given above, adding the same edge correction term:

$$\hat{\rho}(r) = \sum_{i=1}^{n} \sum_{\substack{j=1 \\ (j \neq i)}}^{n} \frac{\mathbf{e}_h\left(r - \left\|\bar{x}_i - \bar{x}_j\right\|\right)}{4\pi r^2 \cdot \text{Vol}\left\{W_{\bar{x}_i} \cap W_{\bar{x}_j}\right\}}. \tag{19}$$

Comparing these equations, the difference is clear: while the Stoyan and Stoyan (1994) version uses the test distance in the denominator, the Raeburn (1996) version (also used by Daniel and Spear, 1999) substitutes in its place the distance between the two crystals under consideration. A number of comparison runs were performed to evaluate the effects of this difference, and the results of the analysis of a nearly completely random simulation are shown in Figure 6. The results show that the Raeburn version will tend to underestimate values for the PCF at small scales, but, because it similarly underestimates the PCF values for the interface-controlled envelope runs, the compensating errors will tend to leave the ultimate conclusions unchanged.

Edge effects

Each of these statistics can be adversely affected when the examination region (a sphere for the L'-function, a spherical shell for the PCF and MCF) intersects the sample boundary. The statistics therefore must be modified to account for these edge effects. Two methods are generally used for this: minus sampling, and window translation.

Minus-sampling method. Minus sampling prohibits calculation for any crystal for which the examination region would intersect the sample boundary (Stoyan and Stoyan, 1994, p. 280). This method can be conceptualized as installing a guard region inside the sample boundary whose thickness is that of the current test distance (Fig. 7). Crystals within this region will not have the examination region centered on them, but may still be counted if they fall within the examination region centered on another crystal not within the guard region. This method has the advantage of introducing the fewest artifacts into the calculation, but requires a large number of crystals, because many are excluded from the calculation, even at small test distances. Additionally, there

is a maximum test distance allowable with this method, although in most cases of present interest, this maximum is greater than the typical test distances of interest for the statistic.

Translation method. The translation method attempts to correct each summand for those crystals missed outside the sample boundary. It divides the summand for each pair of crystals by a factor, $V(W_{Xi} \cap W_{Xj})$, that is the volume of the intersection of the sample boundary offset to two different points: first so that the origin is located at the center of crystal x_i, then so that the origin is located at the center of crystal x_j (Fig. 8a). This is equivalent to the volume of intersection of the sample boundary with a copy offset by the vector from x_i to x_j (Fig. 8b). Dividing each summand in this way causes the summand to increase for crystals that are more widely separated, which tends to compensate for the fraction of the examination region that lies outside the sample boundary. However, because the method does not take into account the degree to which the examination region *actually* lies outside the sample boundary for any particular pair, it is possible in concept for the method to introduce artifacts into the statistics. Nevertheless, as is shown below, the translation method of edge correction produced values very close to those from the minus-sampling method on a suite of crystal simulations, with the advantage of retaining larger numbers of crystals in the analysis.

Previously used statistics

Previously used statistical measures of ordering and clustering are described in Denison *et al.* (1997) and include the ordering index, clustering index and impingement index. The ordering index is derived from the nearest-neighbor test, which evaluates the mean distance to the nearest neighbor of each crystal; discounting volume effects, this index will be greater than unity for an ordered distribution and less than unity for a clustered distribution. The clustering index is derived from the random-point test, which evaluates the mean distance to the nearest crystal center from a random point in the sample; discounting volume effects, this index will be greater than unity for a clustered distribution and less than unity for an ordered distribution. The impingement index is derived from a test that compares the overlap between spherically idealized crystal shapes and the amount of overlap expected in a random distribution; this index will be greater than unity for a clustered distribution and less than unity for an ordered distribution. All three statistics should have a value of unity for a perfectly random distribution of crystal centers. However, these statistics can be altered in complicated ways when applied to arrays of crystals, reflecting complexities introduced by combinations of clustering and ordering effects, volume fraction, and crystal number density, as discussed in Denison *et al.* (1997, p. 38, Fig. 8).

These complexities introduce considerable ambiguity because they can alter the predicted value of each statistic for a given distribution. This makes deductions as to ordering, randomness or clustering (and therefore interfacial or diffusional controls on nucleation and growth) uncertain for any particular value of a given statistic. To reach meaningful conclusions, it has been necessary to consider together all three indices, in combination with numerical simulations of crystallization that produce equivalent textures from known mechanisms.

To ameliorate this ambiguity, in the present work the value of each statistic is calculated for a large number of "envelope" simulations (described in detail below), and the mean and 95%

confidence interval for each statistic is calculated. If the value of the statistic measured on the rock falls outside the confidence interval, then one must reject the randomness hypothesis in favor of either ordering or clustering. This idea is discussed in greater depth below.

Evaluation of correlation functions

It is important when evaluating the utility of a statistical measure to examine its performance on simulations for which the expected value or behavior of the statistic is known. Furthermore, any specific computational implementation should be tested on simulations to prove its ability to produce the correct answers in controlled cases. Here we report such tests on two types of simulations: one type for which the expected results are better constrained, but of less geological relevance, and another type of greater geological relevance, but for which the expected results are less well constrained.

The first type of simulation is an idealization, produced not by modeling crystallization processes, but merely by placing crystals in specific locations, with the restriction that they may not overlap by more than a specific small amount. This allows processing of point arrays whose degrees of ordering and clustering are known. The overlap restriction is designed to broadly mimic restrictions on crystal locations in a rock, although the overlap criterion is somewhat more complex for interface-controlled growth (discussed below) and still more involved for diffusion-controlled growth. The second type is an actual numerical simulation of nucleation and growth of porphyroblasts in a rock, given a specific temperature-time history, and specific rate laws for nucleation and diffusion.

Diagrams

Each data figure in this paper is made up of four diagrams: the L'-function, our proposed variant of the MCF (both calculated using the translation method of edge correction), the PCF calculated using the translation method of edge correction, and the PCF calculated using the minus-sampling method of edge correction. In each case, the horizontal axes represent the test distance, with the lower horizontal axis scaled to the mean radius of the crystals in the sample, and with the upper horizontal axis scaled to the test distance in centimeters; the vertical axis is the value of the statistic. These statistics have differing units, which are generally not included in the literature, as the units have no physical meaning; this convention will be followed here. Each diagram has a data curve (represented by a solid line and point markers) that is plotted along with a pink "envelope." The meaning of the envelope is discussed below, and the method of its calculation is given in Appendix A. Each diagram also shows a horizontal line that represents the value expected for a Poisson distribution of points (zero for the L'-function, unity for the other three). Finally, each diagram has a light blue vertical bar that indicates the range of nearest-neighbor distances for the sample – the center represents the mean, and the width of the bar represents one standard deviation on either side of the mean.

The range of test distances is calibrated to the sample under consideration; in all diagrams the maximum test distance is approximately 6 times the mean nearest-neighbor distance. This is intended to provide rapid calculation times by limiting the number of test distances required,

while ensuring that the data points include the range of separations over which differing crystallization mechanisms are likely to produce discernable effects.

Many data figures are accompanied by three-dimensional renderings of the crystal array in whole or in part from which the data were obtained. These can be clicked to display an interactive 3-D representation using QuickTime for Macintosh or Windows.

Envelope simulations

Each of the various statistical measures mentioned above has a theoretically derived expected value for certain types of point arrays, such as a Poisson distribution. For point-type sample data, one can simply compare the value of the statistic to the expected value to discern trends towards ordering or clustering. However, crystal arrays do not have theoretically derived expected values, because crystals cannot nucleate and grow completely randomly – no crystal may nucleate within another crystal. Expected values of the statistics must accommodate geologically reasonable restrictions on the relative locations of crystal centers, and these restrictions must take into account such factors as nucleation times, growth rates, and the like.

In order to draw conclusions about ordering and clustering trends within a sample data set, we must therefore produce a crystal array that lacks such trends to which we can then compare the sample data set. In order to properly make the comparison, the crystal array should share as many features as possible with the sample data set, aside from the small-scale ordering features that are under examination. The number density of crystals, the size and shape of the sample volume, and the crystal size distribution should be identical in order to maximize confidence in the conclusions drawn from the comparison. Our analysis, presented below, reveals that very great care is required in order to obtain a crystal array to which the sample data can be rigorously compared (cf. Appendix A); previously published attempts at this (Raeburn, 1996; Daniel and Spear, 1999) appear to overlook features that may affect the comparison.

Once a correct crystal array lacking ordering and clustering trends is produced, this array becomes a null-hypothesis case of interface-controlled non-clustered nucleation and growth; if the value of the statistic measured on the sample data set deviates significantly from that measured on the array, then a deviation from the null hypothesis case has been demonstrated. But what constitutes a significant deviation? To answer this question, the Monte Carlo method is used: a large number of null-hypothesis arrays are manufactured, and each statistic is measured on each array. For each statistic, there is a distribution of null-hypothesis values, and one can determine if the sample data falls within a certain distance of the mean of those values. If they do not, one may justifiably conclude, with a corresponding confidence level, that the sample is significantly ordered or clustered relative to a non-clustered interface-controlled case. This is the conceptual basis for our analysis; the details of the production of null-hypothesis, or "envelope" simulations, are given in Appendix A.

The shaded regions on the diagrams presented below represent the 2-σ range or envelope for a set of 100 simulations. If the value of a statistic falls outside the 2-σ envelope, it can be concluded with 95% confidence that the statistic measures significant ordering or clustering relative to non-clustered interface-controlled nucleation and growth. However, if the values fall

within the envelope, then no conclusion can be reached. If it were possible to create a diffusion-controlled envelope for each rock, then one could use that as a second null hypothesis, and test it in order to positively identify interfacial controls on nucleation and growth for data that fell outside that envelope. One published work (Daniel and Spear, 1999) includes an attempt at this, but, as discussed below, the simple simulation of diffusion-controlled nucleation and growth used in the production of the null-hypothesis envelope simulations fails to replicate many of the vital characteristics of the process, and is therefore suspect (cf. Appendix A). One key feature of diffusion-controlled nucleation and growth that the model in Daniel and Spear (1999) fails to replicate is the difference in diffusional domain sizes between crystals of the same size that nucleated at different times and whose diffusional domains impinge upon others at different stages in their growth. In fact, we found in this work that the production of rigorously defensible diffusion-controlled null-hypothesis envelope regions is computationally prohibitive at present.

It is important to note that geologic reasoning must govern the inferences drawn from these data. For example, trends that fall below the null-hypothesis region can only be considered diffusional at scales over which diffusion operates, up to about the mean nearest-neighbor distance. Trends that fall below the null-hypothesis region at scales greater than this must be due to some other cause: for example, the relative sparsity of crystals at scales greater than that of a cluster or layer.

Artificial arrangements of crystals

In order to understand the behavior of correlation functions, a number of simulations were produced and analyzed. The first type of simulation is a completely artificial array of crystal sizes and locations. These crystal arrays exhibited extreme tendencies towards ordering, spatial randomness, or combinations of clustering with ordering or randomness. They are fully detailed in Appendix B, and reveal patterns closely matching predictions based upon characteristics of the crystal arrays. Analysis of these simulations leads to two important results. On one hand, the statistics are quite robust in their ability to detect ordering that has been disturbed by random permutations. On the other hand, clustering of crystals can strongly obscure indicators of small-scale ordering that might be diagnostic of diffusion-controlled growth. The L'-function and PCF are more susceptible to degradation of the diffusional signal than is the MCF, but as the scale of clustering effects approaches the scale of diffusional effects (roughly half the mean nearest-neighbor distance), all of these functions lose their ability to extract an underlying diffusional ordering signal from a clustered array of crystals.

Simulations of nucleation and growth

The second type of simulation is more sophisticated and is produced by numerical modeling of a nucleation-and-growth process, with time as an explicit variable (Carlson *et al.*, 1995). A number of these types of simulations have been produced and analyzed. Four are described below: each is either interface-controlled or diffusion-controlled, with or without layering effects induced by a spatially sinusoidal probability of nucleation in one dimension with uniform nucleation probability in the other two dimensions, or clustering effects induced by spatially sinusoidal probability of nucleation in three dimensions.

Interface-controlled, uniform distribution. The interface-controlled case is the default distribution, and this was analyzed to ensure that the statistics can reproduce the expected values. An interface-controlled simulation was produced that includes an exponential increase in the rate of nucleation with time. There are 1739 crystals in a 1-cm^3 cube. As expected, the values for the correlation functions all fall within the interface-controlled envelope (Fig. 9).

Interface-controlled with layers. An interface-controlled simulation similar to that shown in Figure 9 was produced, except with layering on a scale of 0.5 cm. This would correspond to interface-controlled nucleation and growth in a layered sample. The simulation has three distinct layers in a 1-cm^3 cube. The results are shown in Figure 10 with a rendering of a sub-volume. As expected, the data show clustering up to about 10 mean radii (~0.2 cm), and fall below the envelope at greater length scales, reflecting the relative sparsity of crystals beyond the scale of layering. There is no evidence of growth suppression in the MCF data.

Interface-controlled with clustering. A more complex interface-controlled simulation was also produced (Fig. 11), except with clustering on a scale of about 1 cm. The clustering is achieved by imposing a sinusoidal probability of nucleation in three dimensions. The data show the effects of clustering in the L'-function and the PCF, almost completely obscuring the interface-controlled signature. However, the MCF shows the sample data fall within the null hypothesis region, as expected from the clustering algorithm, which only varies nucleation probability, and not growth rates.

Diffusion-controlled, uniform distribution. Previous work has shown regional-metamorphic samples from a range of rock types and localities to have grown in diffusion-controlled nucleation and growth environments (Carlson, 1989, 1991; Carlson and Denison, 1992; Carlson *et al.*, 1995; Denison and Carlson, 1997). In order to demonstrate that the statistics give the correct results in such circumstances, a diffusion-controlled simulation was produced that includes an exponential increase in nucleation with time, together with diffusional suppression of nucleation and growth, using the simulation model of Carlson *et al.* (1995). The volume fraction of porphyroblasts is 0.1, and there are 1919 crystals in a 1-cm^3 cube. The results for this simulation are shown in Figure 12. As expected, at scales up to about the mean nearest-neighbor distance, the values for the correlation functions fall below the interface-controlled envelope. The MCF shows suppression of growth up to about twice the mean nearest-neighbor separation. The larger scale of growth suppression is consistent with expectation, because a crystal's growth is inhibited not only by its nearest neighbor (as is the case with its nucleation) but also by more distant neighbors with which its diffusional domain impinges over the course of its growth.

Diffusion-controlled with layers. If the sample analyzed above were layered, as might be common for metasedimentary rocks, then the statistics should reveal ordering within clustering. In order to test this, a diffusion-controlled simulation was produced that includes an exponential increase in nucleation with time, together with diffusional suppression of nucleation and growth. The volume fraction of porphyroblast material is 0.1, and there are 3059 crystals in a 1-cm^3 cube. The model parameters are the same as the diffusion-controlled simulation above, save for an increased nucleation rate, an extended period of heating and a sinusoidal distribution of nucleation probability in which the sine curve has a wavelength of 0.33, producing three layers in the sample. The results for this simulation are given in Figure 13, together with a rendering of

a sub-volume. The data show ordering at small scales, up to about the mean nearest-neighbor distance. Ordering is also present at scales greater than 0.15 cm or 0.20 cm, reflecting the periodicity of the layering (crystals are sparse at $x = 0$, $x = 0.5$, and $x = 1.0$, so the mean distance to a sparse region is about 0.18 cm). The MCF results for this simulation should be regarded skeptically, because the nature of the simulated layering is not geologically reasonable: it only involves an inhomogeneous distribution of nucleation sites, not nutrients, leading to abnormally large crystals at the border between the dense and sparse layers, as is evident from Figure 13a.

Tests of robustness of correlation functions

Denison *et al*. (1997, Appendix 1) described limitations on sample characteristics for three single-valued statistics: the ordering index, clustering index, and impingement index. They conclude that because of edge effects, a minimum of 1000 crystals is necessary to obtain reliable values for these statistics. A similar set of analyses was performed to evaluate appropriate sample sizes for application of correlation-function statistics. These results are described in Appendix C, and demonstrate that correlation functions are significantly more robust that single-valued statistics. The tests suggest that correlation functions may produce reliable results from data sets as small as a few hundred crystals, although greater numbers will greatly strengthen the confidence that can be placed in the inferences drawn.

Application to natural samples

Denison and Carlson (1997) raised the problem that the three single-valued statistics used by them are all interdependent, and so a single numerical boundary for each that would separate diffusional from interfacial control in a sample does not exist. To address this issue, correlation functions were used to reanalyze the rocks studied by Denison and Carlson (1997), comprising seven samples from three localities, representing a range of rock types and metamorphism-deformation relationships. The previously used statistics were also calculated for the samples and their interface-controlled envelopes. These samples are presented as an application for the correlation functions, and therefore are not described in detail here; for detailed descriptions, see Denison and Carlson (1997, p. 46).

Picuris Mountains suite

Two samples (PM1, PM2) from the Picuris Mountains of north-central New Mexico were re-analyzed, together with the diffusion- and interface-controlled simulations that were designed to model the crystallization of each sample. The rock samples and simulation parameters are described in detail in Denison and Carlson (1997). These samples are garnetiferous quartzites in which garnet growth was post-kinematic. Sample PM2 was originally scanned simultaneously with two other samples, resulting in only a small usable analysis volume (1772 crystals in 13.8 cm^3, with a large aspect ratio).

The data for Sample PM1 are shown in Figure 14. The data show excursions below the interface-controlled 2-σ envelope up to scales on the order of the mean nearest-neighbor distance for the L' -function and PCF, and up to about twice that distance for the MCF. This is to be expected, and is in good agreement with the conclusions from the single-valued statistics.

The results for the single-valued statistics were obtained in Denison and Carlson (1997), and are given in Table 1, together with the 2-σ bounds from the envelope simulations. This comparison confirms the results previously obtained with these statistics, in that the rock data, with only one exception, show either ordering or clustering. The time-explicit interface-controlled nucleation and growth simulations tend to fall between the 2-σ null-hypothesis values, but because many of these simulations incorporate explicit spatially varying probabilities for nucleation, they should not be expected to fall between the 2-σ values, just as the similar interface-controlled simulation of Figure 11 falls outside the envelope. Significantly, the values of the indices may fall on either the ordering or clustering side of the envelope, just as in Figure 11, the data fall above or below the envelope at different scales. The diffusion-controlled time-explicit nucleation and growth simulations, with only three exceptions, fall outside the null-hypothesis bounds. However, because these simulations generally incorporate explicit clustering of nucleation sites that are not shared by the null-hypothesis simulations, we can in a strict sense have no expectation as to whether the single-valued statistics will fall within, above, or below, the null-hypothesis range.

The data for sample PM2 are shown in Figure 15. They differ from sample PM1 in that the excursions below the interface-controlled envelope are not as pronounced for the location-based statistics, although the MCF still shows a strong growth-suppression signal. This confirms the diffusion-controlled conclusion, and suggests that diffusional control was operating during the crystallization of PM2, but that clustering of nucleation sites (probably due to inhomogeneities in the precursor) tends to obscure the ordering signal.

Mica Dam sample

Sample MD is from a locality near the dam along Mica Creek in British Columbia. It is a pelite in which garnet growth was syn-kinematic; it is also compositionally heterogeneous and has kyanite porphyroblasts in addition to the garnet. Functional values for sample MD are shown in Figure 16. The functions indicate diffusional control at scales up to about the mean nearest-neighbor distance, although the signal is again weak.

The data for this sample illustrate the different sensitivities of the MCF and the other correlation functions: the L'-function and the PCF show that the ordering of nucleation sites is barely discernable, presumably due to clustering of these sites as a result of initial inhomogeneities in the precursor. In contrast, the MCF shows a strong signal below the envelope values, indicating significant suppression of growth as a result of diffusional competition for nutrients.

Whitt Ranch suite

A suite of four samples (WR1, WR2, WR3, WR4) from the Whitt Ranch near Babyhead in central Texas was also reanalyzed. These samples are of mafic composition and appear nearly homogeneous at hand-sample scale. In these rocks, the garnets are thought to have crystallized syn-kinematically, but in structural settings with limited penetrative deformation.

The data for samples WR1-WR4 are shown in Figures 17-20. All show diffusional suppression of nucleation at scales up to about the mean nearest-neighbor distance, and diffusional suppression of growth to about twice that distance. Samples WR3 and WR4 also show significant clustering at scales greater than about one mean nearest-neighbor distance.

Conclusions

Building upon prior work (Raeburn, 1996; Daniel and Spear, 1999), the analysis presented here identifies several improvements to methods that employ correlation functions for textural analysis. A corrected formulation of the Pair Correlation Function is presented in Equation (19). An unbiased Mark Correlation Function is presented in Equation (16), which provides a more conservative assessment of the significance of size-isolation correlations. These spatial correlation functions are seen to exhibit a range of comprehensible behaviors when applied to artificial crystal arrays, knowledge of which increases our ability to properly interpret features that arise when the functions are applied to natural samples. We advocate careful testing of any particular calculation scheme for these functions against a series of crystal arrays with predetermined textural characteristics, both artificial arrays that yield known outcomes and arrays produced by numerical simulations of crystallization processes. In particular, our results highlight the importance of constructing null-hypothesis envelopes with great rigor, as emphasized by: (a) the possibility of spurious indications of diffusional control when observability criteria are ignored (Fig. A1); and (b) the failure of previous attempts at constructing diffusion-controlled null-hypothesis envelopes to encompass the characteristics of crystal arrays produced by numerical simulation of diffusion-controlled crystallization (Fig. A2). While not disproving earlier analyses that omitted these refinements, these results suggest that data sets from earlier studies should be re-analyzed to include these improvements in technique.

When properly and carefully applied, correlation functions are a powerful adjunct to other statistical measures and methods of textural analysis. For analysis of small numbers of crystals and samples of high aspect ratio, they have the advantage of being more robust than the single-valued statistics used previously. They also have the ability in some cases to elucidate superposed ordering and clustering effects at different scales in a single sample. It is important to note, however, that even when these functions are used, clustering may obscure the underlying mechanistic signal. As this signal may be either ordered or random, clustered arrays may originate under either interfacial or diffusional control, and in such arrays the textural evidence that allows discrimination between the two possibilities may be obscured. For this reason, spatial correlation functions should be used in conjunction with other statistical measures, with chemical analysis of growth zoning, if preserved, and with models of nucleation and growth processes to discern the underlying controls on the crystallization of metamorphic porphyroblasts.

The results derived from this study corroborate those of Denison and Carlson (1997), who used single-valued statistics along with radius-rate data and diffusional-domain analysis to demonstrate diffusional control in a range of samples. Our careful use of correlation functions confirms their findings; this consistency highlights the utility and reliability of both types of statistics, and the agreement of inferences from both methods emphasizes the geological conclusion reached earlier – diffusional processes were the controlling factors in the nucleation and growth of the garnet porphyroblasts in these rocks. This finding suggests that prior

identifications of interface-controlled crystallization (Raeburn, 1996; Daniel and Spear, 1999) or diffusion-controlled crystallization (Carlson, 1989, 1991; Carlson and Denison, 1992; Denison and Carlson, 1997; Denison *et al.*, 1997) are not artifacts of the statistical methods used, but instead reveal genuine differences in environmental variables that control crystallization mechanisms for garnet.

Acknowledgements

References cited

Avrami, M. (1940) Kinetics of phase change. II: Transformation-time relations for random
     distribution of nuclei. Journal of Chemical Physics, 8, 212-224.
Carlson, W. D. (1989) The significance of intergranular diffusion to the mechanisms and kinetics
     of porphyroblast crystallization. Contributions to Mineralogy and Petrology, 103, 1-24.
Carlson, W. D. (1991) Competitive diffusion-controlled growth of porphyroblasts. Mineralogical
     Magazine, 55, 317-330.
Carlson, W. D. and Denison, C. (1992) Mechanisms of porphyroblast crystallization: Results
     from high-resolution computed X-ray tomography. Science, 257, 1236-1239.
Carlson, W. D., Denison, C. and Ketcham, R. A. (1995) Controls on the nucleation and growth
     of porphyroblasts; kinetics from natural textures and numerical models. Geological Journal,
     30, 207-225.
Carmichael, D. M. (1969) On the mechanism of prograde metamorphic reactions in quartz-
     bearing pelitic rocks. Contributions to Mineralogy and Petrology, 20, 244-267.
Cressie, N. A. C. (1993) Statistics for spatial data. J. Wiley, New York.
Daniel, C. G. and Spear, F. S. (1999) The clustered nucleation and growth processes of garnet in
     regional metamorphic rocks from north-west Connecticut, USA. Journal of Metamorphic
     Geology, 17, 503-520.
Denison, C. and Carlson, W. D. (1997) Three-dimensional quantitative textural analysis of
     metamorphic rocks using high-resolution computed X-ray tomography. Part II: Application
     to natural samples. Journal of Metamorphic Geology, 15, 45-57.
Denison, C., Carlson, W. D. and Ketcham, R. A. (1997) Three-dimensional quantitative textural
     analysis of metamorphic rocks using high-resolution computed X-ray tomography. Part I:
     Methods and techniques. Journal of Metamorphic Geology, 15, 29-44.
Fisher, G. W. (1978) Rate laws in metamorphism. Geochimica et Cosmochimica Acta, 42, 1035-
     1050.
Hirsch, D. M. and Carlson, W. D. (1997) Correlation functions support diffusion-controlled
     garnet crystallization in a range of regional metamorphic samples. GSA Abstracts with
     Programs, 29, A-338.
Joesten, R. L. (1991) Kinetics of coarsening and diffusion-controlled mineral growth. Reviews in
     Mineralogy, 26, 507-582.
Kerrick, D. M., Lasaga, A. C. and Raeburn, S. P. (1991) Kinetics of heterogeneous reactions.
     Reviews in Mineralogy, 26, 583-671.
Konig, D., Carvajal-Gonzalez, S., Downs, A. M., Vassy, J. and Rigaut, J. P. (1991) Modeling
     and analysis of 3-D arrangements of particles by point processes with examples of
     application to biological data obtained by confocal scanning light microscopy. Journal of
     Microscopy, 161, 405-433.
Kretz, R. (1973) Kinetics of the crystallization of garnet at two localities near Yellowknife.
     Canadian Mineralogist, 12, 1-20.
Kretz, R. (1974) Some models for the rate of crystallization of garnet in metamorphic rocks.
     Lithos, 7, 123-131.
Kretz, R. (1994) Metamorphic crystallization. J. Wiley, Chichester, Sussex, England; New York.
Raeburn, S. P. (1996) New methods in quantitative metamorphic petrology. Unpub. Ph.D.
     Thesis, Pennsylvania State University.

Ridley, J. and Thompson, A. B. (1986) The role of mineral kinetics in the development of metamorphic microtextures. In J. V. Walther, B. J. Wood and S. K. Saxena, Eds., Fluid-rock interactions during metamorphism, 154-193, Springer-Verlag, New York.

Ripley, B. D. (1976) The second-order analysis of stationary point processes. Journal of Applied Probability, 13, 255-266.

Ripley, B. D. (1981) Spatial statistics. Wiley, New York.

Rubie, D. C. (1998) Disequilibrium during metamorphism; the role of nucleation kinetics. In P. J. Treloar and P. J. O'Brien, Eds., What drives metamorphism and metamorphic relations?, 199-214, Geological Society, London.

Rubie, D. C. and Thompson, A. B. (1985) Kinetics of metamorphic reactions at elevated temperatures and pressures; an appraisal of available experimental data. In A. B. Thompson and D. C. Rubie, Eds., Metamorphic reactions; kinetics, textures, and deformation, 27-79, Springer-Verlag, New York.

Spry, A. (1969) Metamorphic textures. Pergamon Press, Oxford.

Stoyan, D. and Stoyan, H. (1994) Fractals, random shapes, and point fields: methods of geometrical statistics. Wiley, Chichester; New York.

Walther, J. V. and Wood, B. J. (1984) Rate and mechanism in prograde metamorphism. Contributions to Mineralogy and Petrology, 88, 246-259.

Table 1. OI, CI, II for all samples, DC sims and IC sims Single-valued statistical indices for studied samples and corresponding diffusion- and interface-controlled simulations, together with 2-σ confidence regions for 100 interface-controlled null-hypothesis runs, and conclusion of significant deviation from null-hypothesis (interfacial control). Values that exceed the 2-σ envelope bounds are ordered for the ordering and clustering indices, and clustered for the impingement index. Values that fall below the 2-σ envelope bounds are clustered for the ordering and clustering indices, and ordered for the impingement index. The values given here differ slightly from those in Denison and Carlson (1997) because these represent re-analysis using a sample sub-volume in the shape of a rectangular prism, in contrast to the convex hull used previously to make up the sample bounding box.

| | Ordering Index | | | | Clustering Index | | | | Impingement Index | | | |
| | | 2-σ Env. | | | | 2-σ Env. | | | | 2-σ Env. | | |
Rock/Sim	Value	Min	Max	Result[1]	Value	Min	Max	Result	Value	Min	Max	Result
PM1	1.25	1.07	1.09	O	0.94	0.98	1.04	O	0.82	0.93	0.95	O
DC Sim.	1.13	1.05	1.10	O	1.10	0.99	1.08	C	0.90	0.75	0.75	C
IC Sim.	1.13	1.02	1.04	O	1.01	1.00	1.09		0.99	0.98	1.03	
PM2	1.06	0.98	1.02	O	1.14	1.05	1.14	C	0.97	0.98	0.99	O
DC Sim.	0.95	0.99	1.06	C	1.80	1.05	1.19	C	0.94	0.87	0.87	C
IC Sim.	0.99	0.98	1.03		1.80	1.04	1.15	C	1.09	0.98	1.02	C
WR1	1.12	1.00	1.05	O	1.03	1.04	1.17	O	0.90	0.95	0.98	O
DC Sim.	1.11	1.00	1.07	O	1.16	1.05	1.21		0.92	0.86	0.86	C
IC Sim.	1.00	1.01	1.04	C	1.25	1.01	1.08	C	1.04	0.98	1.02	C
WR2	1.24	1.06	1.09	O	0.91	0.97	1.03	O	0.79	0.92	0.94	O
DC Sim.	1.16	1.01	1.10	O	1.00	1.02	1.19	O	0.87	0.75	0.77	C
IC Sim.	1.03	1.03	1.05		1.01	0.99	1.04		0.99	0.97	1.01	
WR3	1.24	1.04	1.06	O	0.91	1.00	1.06	O	0.87	0.95	0.96	O
DC Sim.	1.15	1.03	1.07	O	1.00	0.99	1.06		0.91	0.85	0.85	C
IC Sim.	1.03	1.02	1.04		1.01	0.99	1.05		1.00	0.98	1.01	
WR4	1.21	1.04	1.05	O	0.99	0.99	1.05	O	0.87	0.95	0.96	O
DC Sim.	1.06	1.01	1.05	O	0.85	1.01	1.10	O	0.94	0.88	0.88	C
IC Sim.	1.02	1.01	1.03		1.02	1.00	1.04		0.99	0.98	1.00	
MD	1.03	0.91	1.01	O	1.21	1.06	1.33		0.96	0.98	1.00	O
DC Sim.	1.04	0.92	1.02	O	1.30	1.09	1.31		0.97	0.96	0.96	C
IC Sim.	1.01	0.96	1.01	O	1.22	1.07	1.22	C	0.99	0.98	1.02	

[1]O = ordered, C = clustered
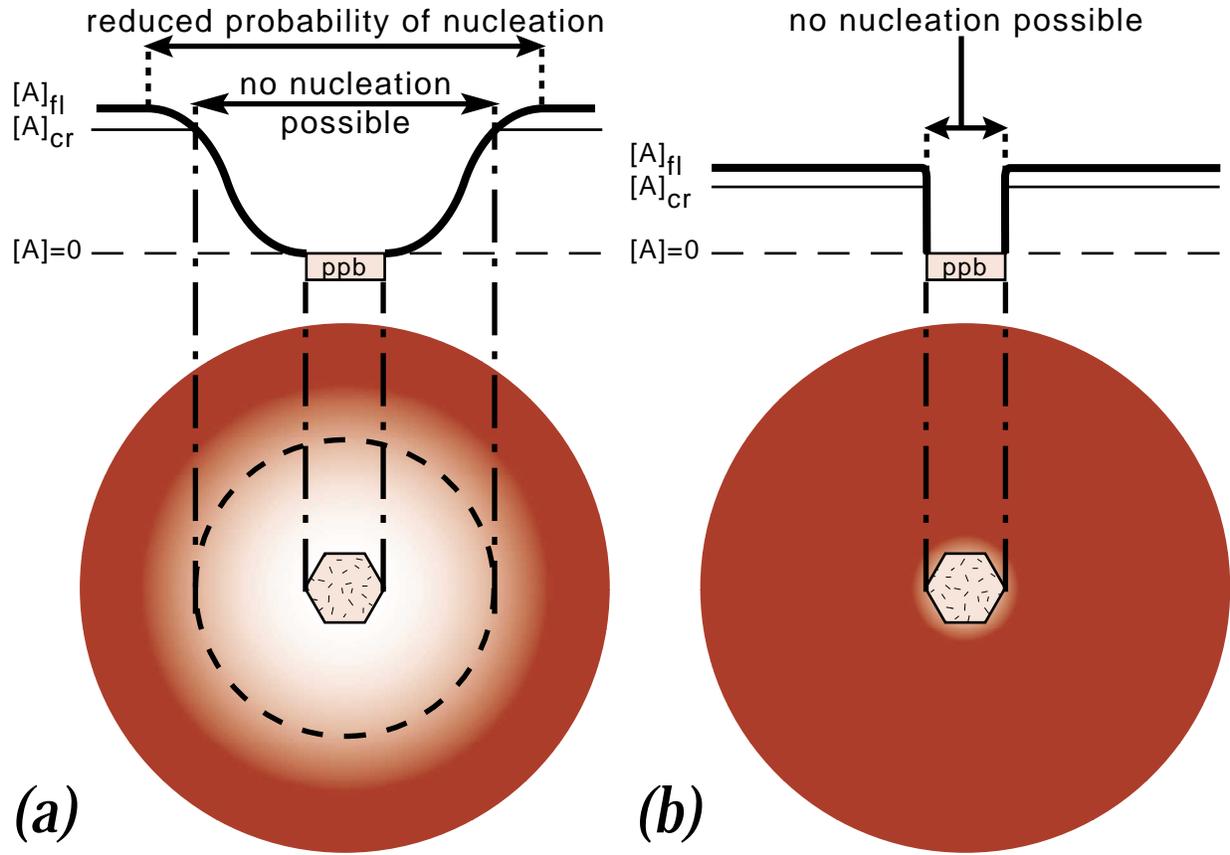
Figure 1. Schematic 2-D illustration of diffusion-controlled suppression of nucleation in the vicinity of a growing porphyroblast ("ppb"), after Carlson (1989). (a) If diffusion is sluggish relative to interfacial reaction, then near a growing porphyroblast slow diffusion produces gradients in the chemical affinity for the crystallization reaction in the intergranular fluid $[A]_{fl}$. This results in zones of zero probability of nucleation where the intergranular chemical affinity is less than the critical value required to overcome the activation energy for nucleation $[A]_{cr}$. These zones are surrounded by zones of reduced probability of nucleation where the chemical affinity is less than the value in regions unaffected by diffusion, but greater than the critical value. (b) If diffusion is rapid, then the only significant effect is the prevention of nucleation within the volume of a pre-existing porphyroblast.
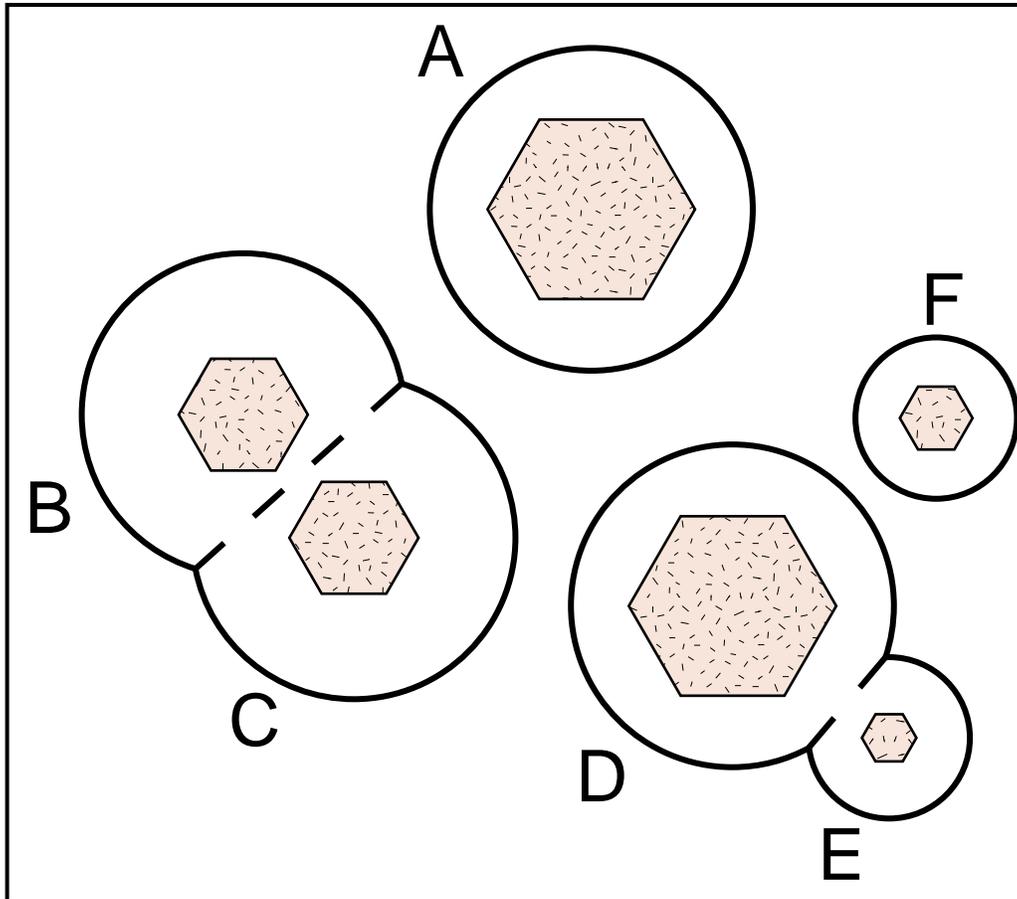
Figure 2. Schematic 2-D illustration of diffusion-controlled retardation of growth in the vicinity of a growing porphyroblast, after Carlson (1991). Competition for nutrients among closely-spaced porphyroblasts reduces the growth rates for crystals in close proximity to each other (B and C) relative to that for an isolated crystal (A) that nucleated at the same time. A crystal (E) that nucleates near the edge of the diffusionally-depleted zone of a pre-existing crystal (D) will initially have minor effects on the growth rate of the pre-existing crystal, but will itself grow more slowly than an isolated crystal that nucleated at the same time (F). Surfaces of impingement between adjacent depleted zones are the boundaries of diffusional domains; their approximate locations are marked by broken lines.
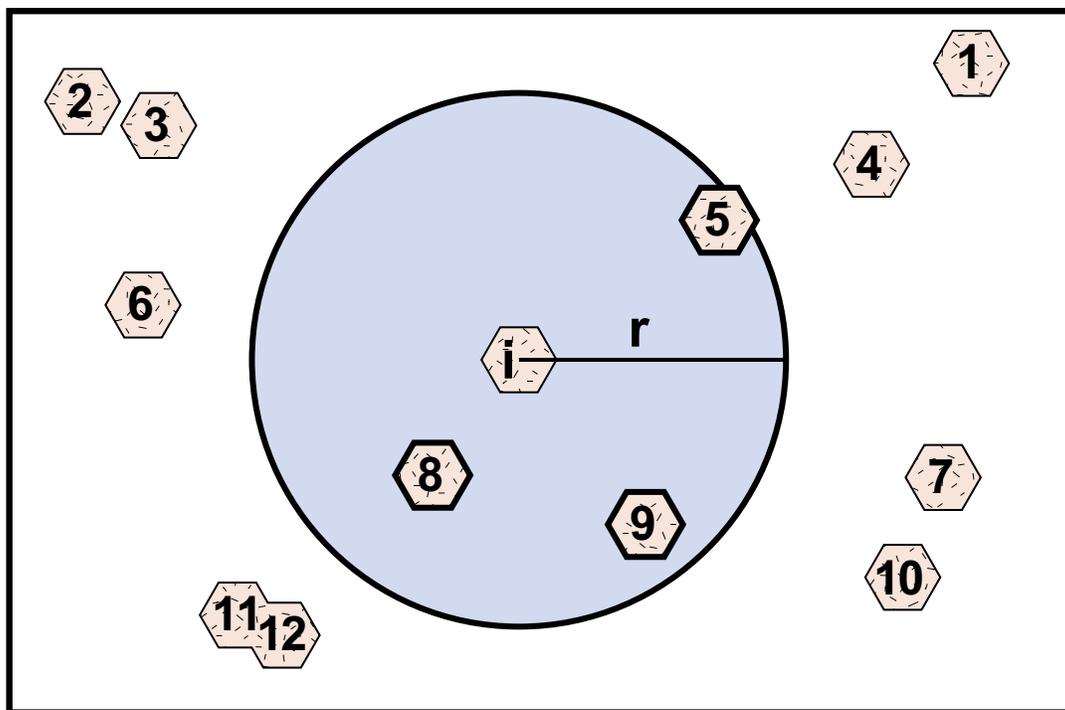
Figure 3. Schematic 2-D illustration of measurement regions for the *K*, *L*, and *L'* functions. For each crystal *i* in the sample, each other crystal *j* whose center lies within a sphere of radius *r* (shaded circle) centered at crystal *i* is counted. In this illustration, the crystals outlined in bold (*j*=5, *j*=8, and *j*=9) will be counted in the summand for crystal *i*; the others will not.
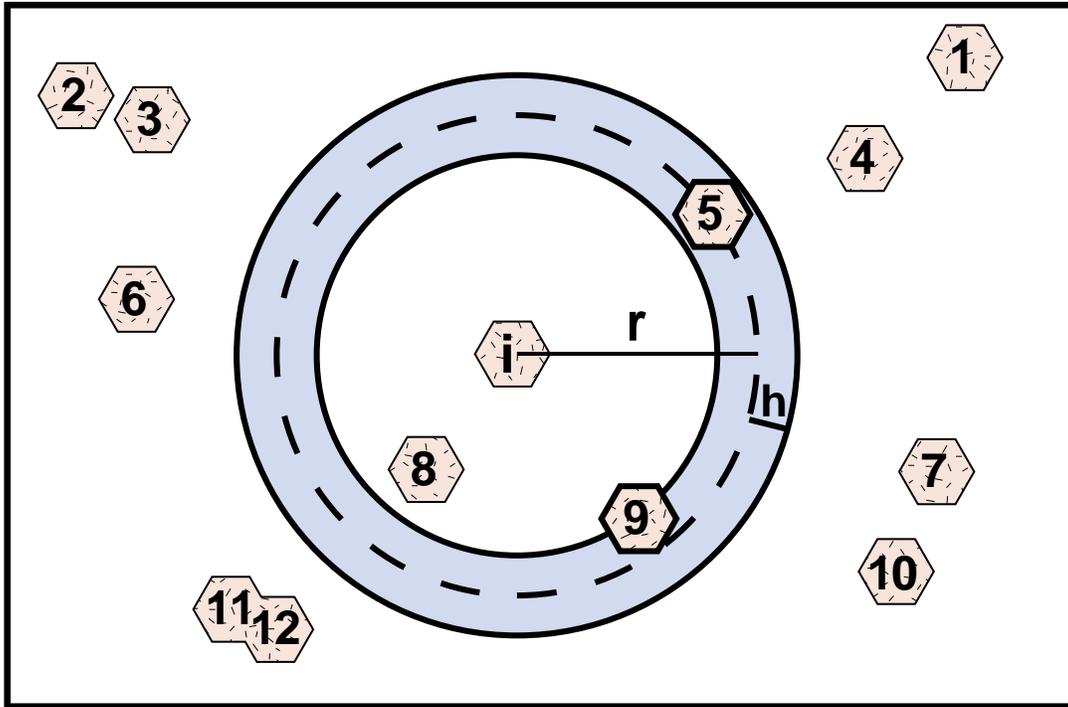
Figure 4. Schematic 2-D illustration of measurement regions for the Pair Correlation and Mark Correlation Functions. For each crystal i in the sample, each other crystal j whose center lies within a spherical annulus (shaded ring) of thickness $2h$ and radius r centered at crystal i is counted. In this illustration, the crystals outlined in bold ($j=5$, and $j=9$) will be counted in the summand for crystal i; the others will not.
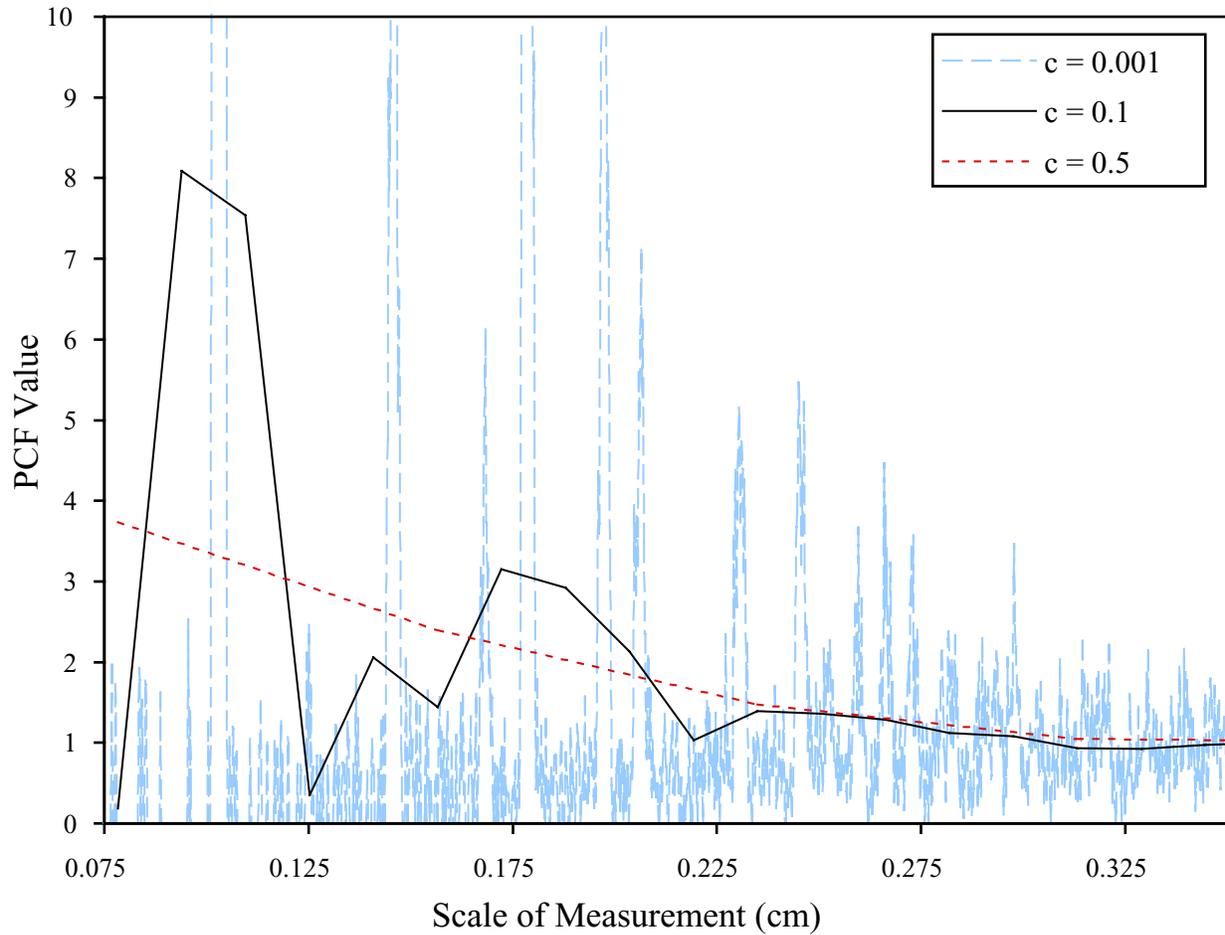
Figure 5. Illustration of the effect of varying bandwidth in the Epanecnikov kernel function on the Pair Correlation Function curve. Each of the four curves represents a re-analysis of the same data set (also analyzed in Figure B7), varying only the value of c in order to alter the bandwidth. Larger values of the bandwidth $h = c \, \lambda^{-1/2}$ produce smoother curves; excessive smoothing from too large a bandwidth results in a loss of textural information. At small values of the bandwidth h, there are scales of measurement for which the calculation does not include any crystals.
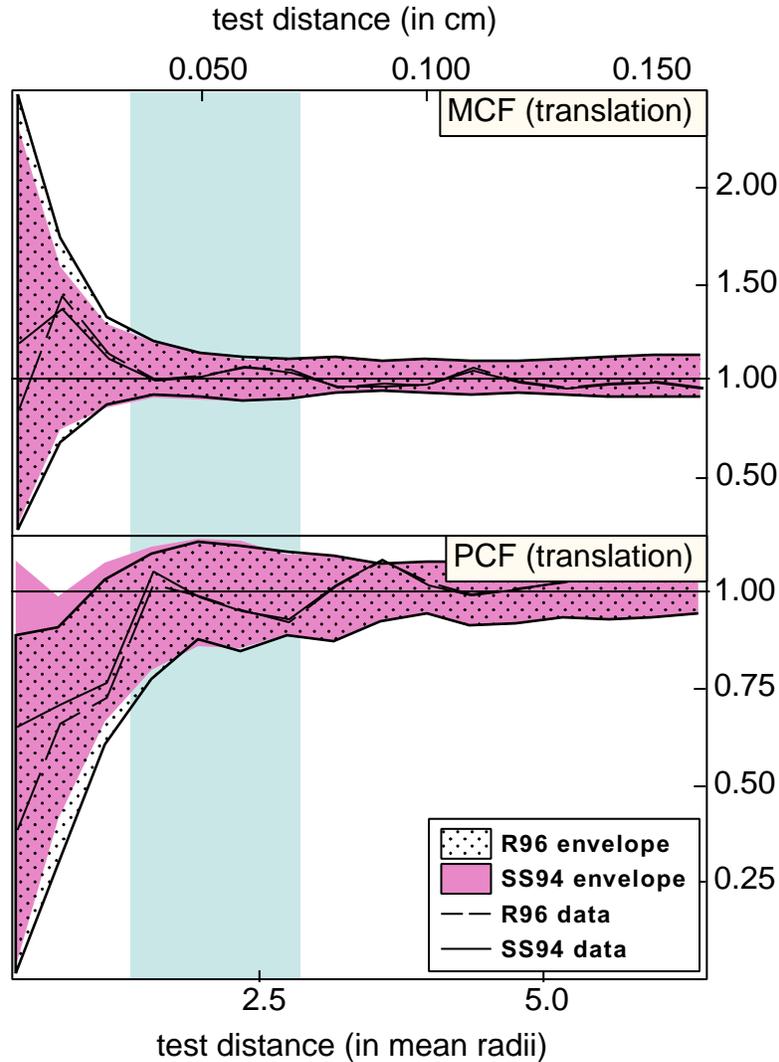
Figure 6. Comparison between the present versions of the MCF and PCF (taken from Stoyan and Stoyan, 1994, "SS94") and those proposed by Raeburn (1996), "R96", performed on the random simulation given in Figure 9. The Raeburn statistic is systematically slightly lower than the present version, particularly at small test distances, but because it is also used to measure the envelopes, compensating errors may leave the conclusion unchanged.
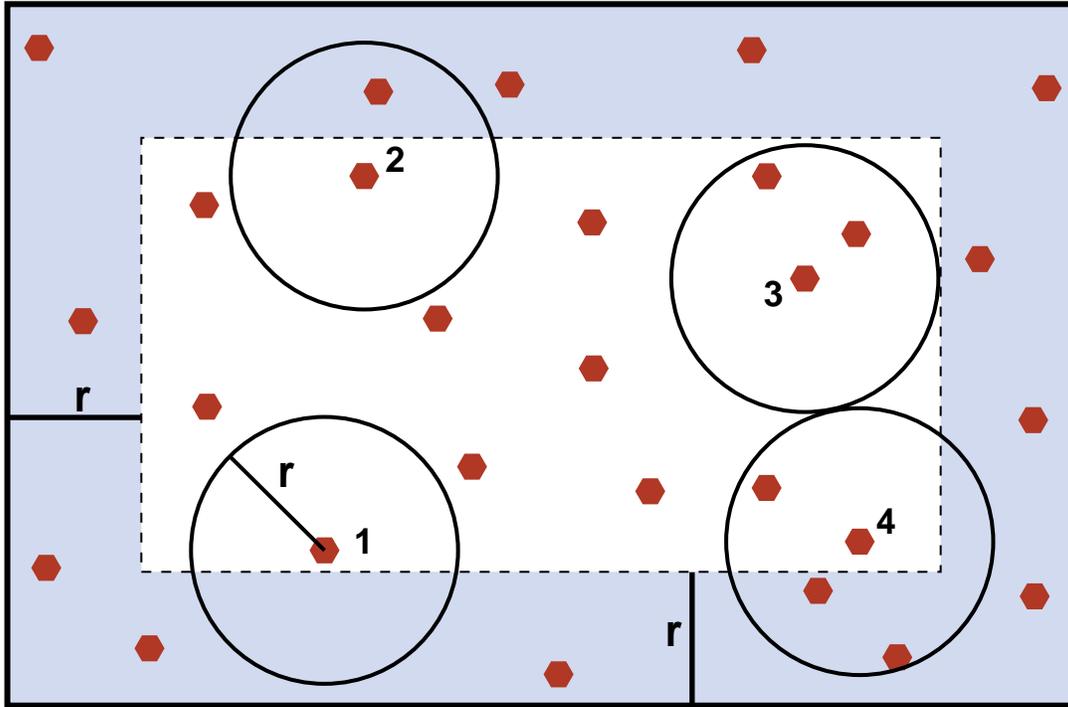
Figure 7. Schematic 2-D illustration of "minus-sampling" edge-correction method. A guard region (wide shaded border region) of the same thickness as the test distance, r, is placed inside the sample boundary. The iteration over crystals i (placement of measurement region) is prohibited from this region, although they may be counted as crystals j within measurement regions. This effectively prohibits the measurement regions from ever intersecting the sample boundary. Four allowable measurement regions are shown as solid circles.
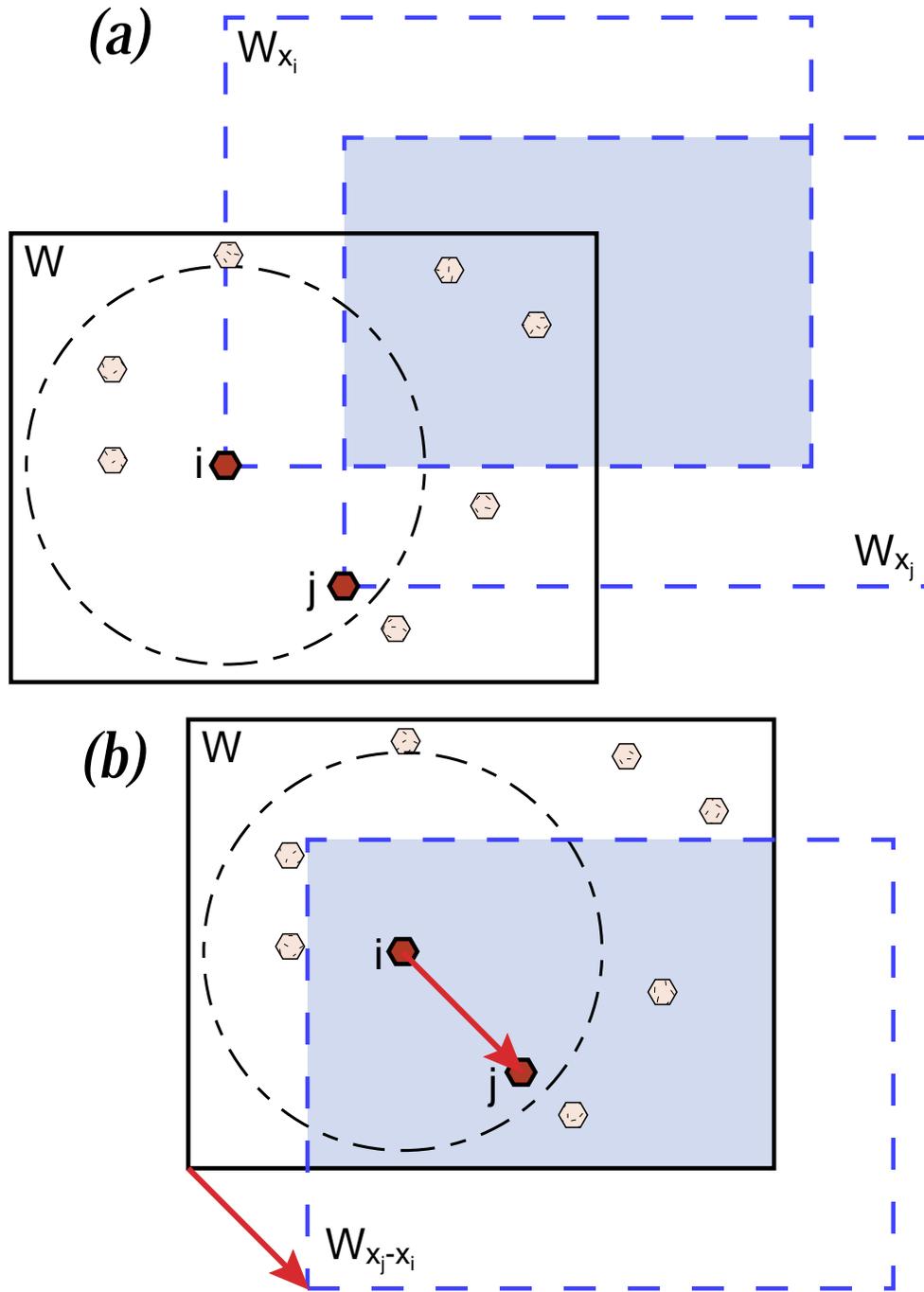
Figure 8. Schematic 2-D illustration of translation edge-correction method. For the pair of crystals in bold, i and j, the summand is divided by the volume of the shaded region. (a) As defined in Stoyan and Stoyan (1994), this region is $W_{x_i} \cap W_{x_j}$, the intersection of the sample region W offset to each of the crystals in the pair. (b) This volume is equivalent to $W \cap W_{x_j-x_i}$, the intersection of the sample region W and that region offset by the vector from the center of crystal i to the center of crystal j. The value of the summand is normalized by this intersection volume for each pair counted.
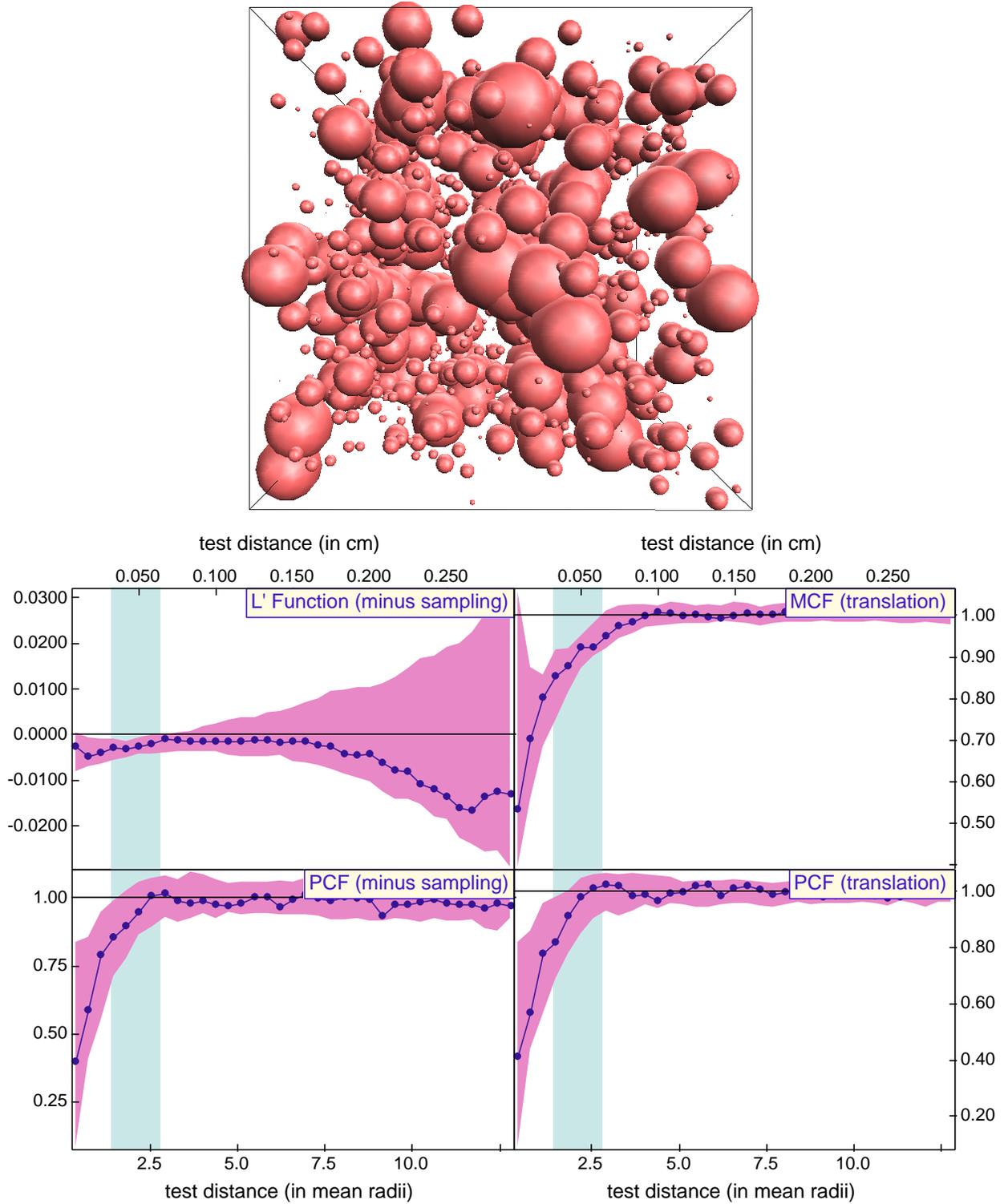
Figure 9. (a) Rendering of sub-volume of simulation IC-2, a thermally accelerated interface-controlled nucleation and growth simulation of 1739 crystals. (b) Correlation functions measured on this simulation; data fall within the 2-σ envelope, as expected.
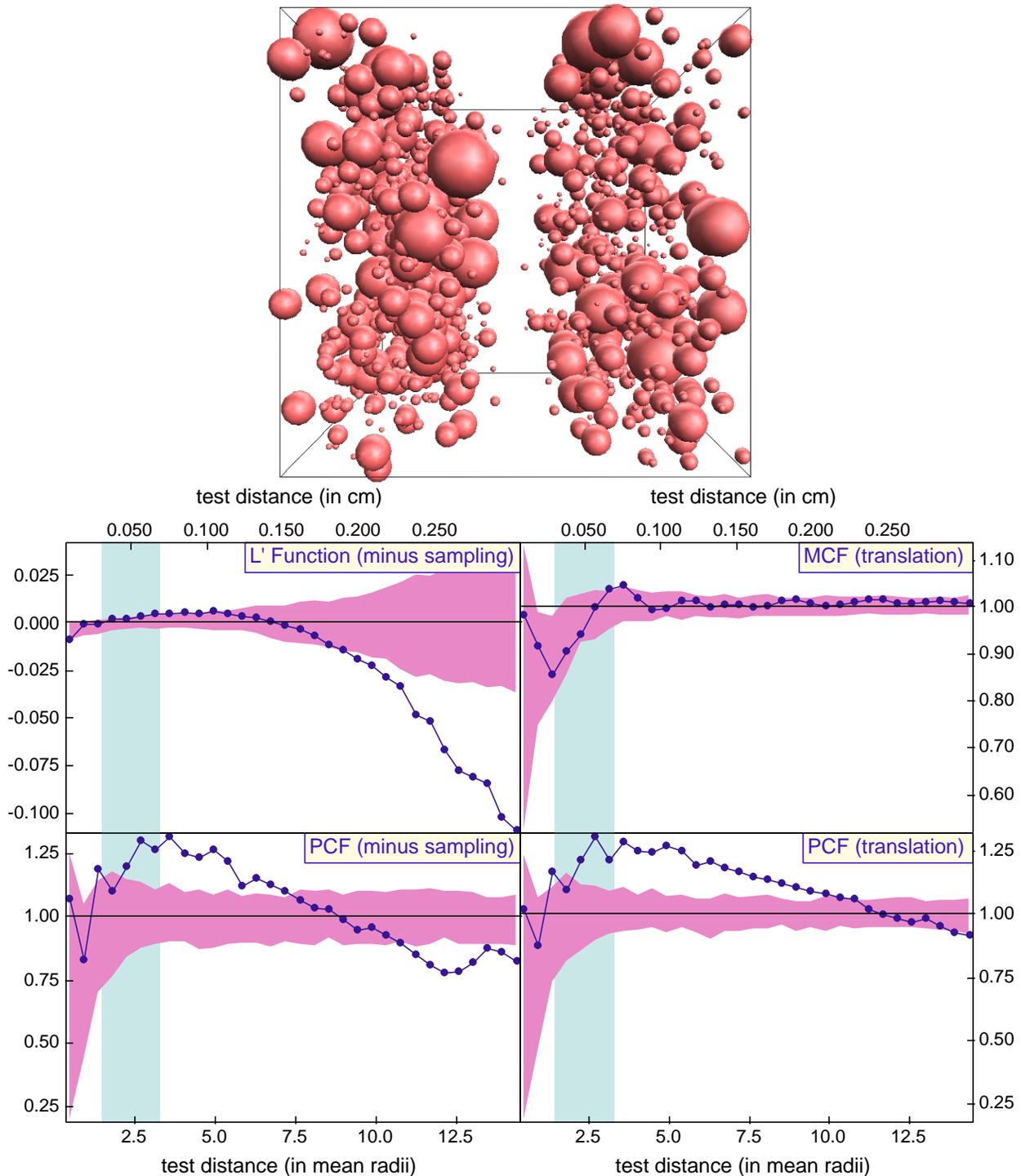
Figure 10. (a) Rendering of sub-volume of layered simulation IC-L2, in which layering is induced by a sinusoidal nucleation probability in one dimension imposed on a simulation of thermally accelerated interface-controlled nucleation and growth. (b) Results of correlation functions measured on this layered array of 1172 crystals. Data show clustering up to about 10 mean radii (~0.2 cm), and fall below the 2-σ envelope at greater length scales, reflecting the relative sparsity of crystals beyond the scale of layering; the MCF data show no growth suppression, as expected from input parameters of simulation IC-L2.
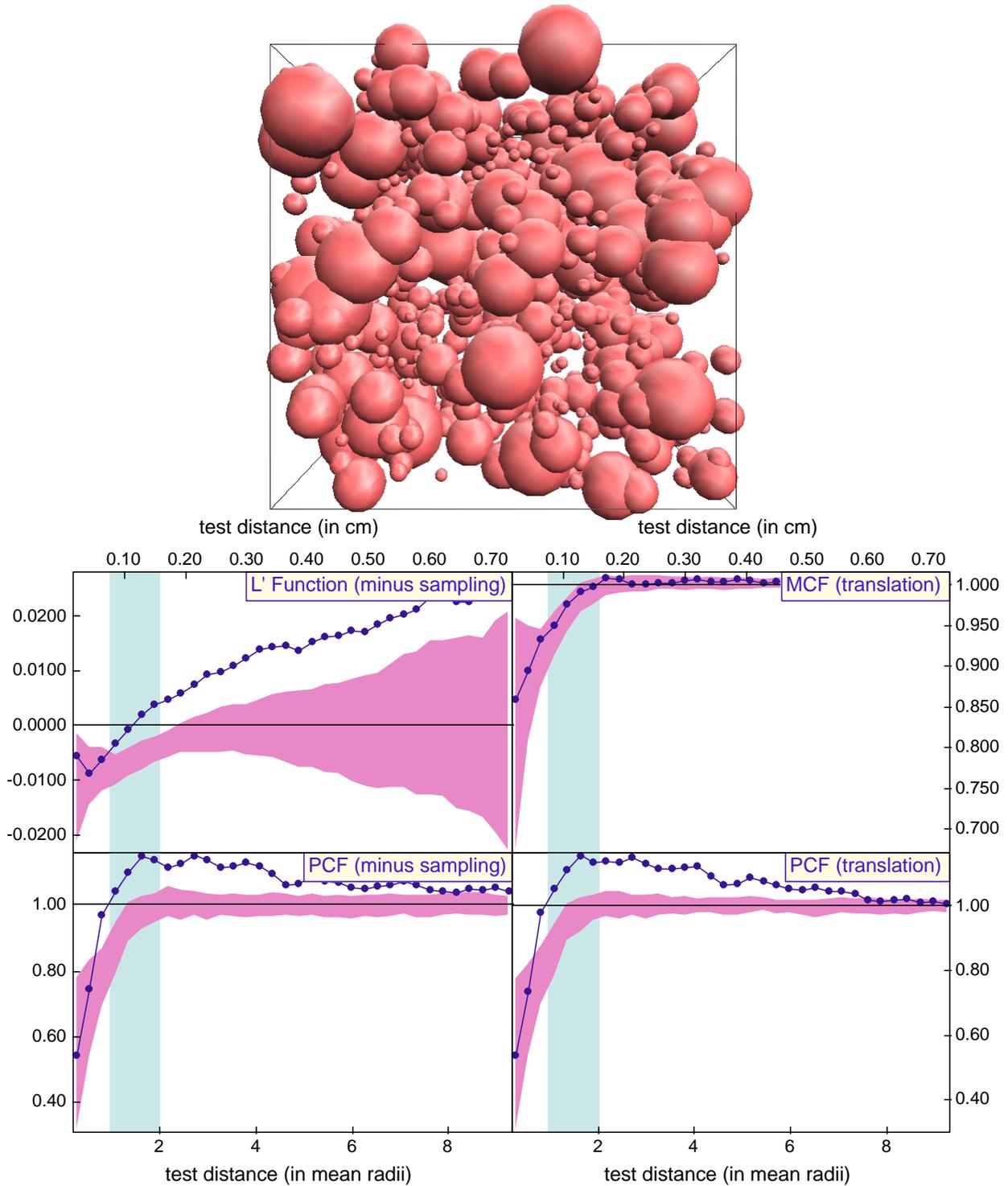
Figure 11. (a) Rendering of simulation IC-WR1, a thermally accelerated interface-controlled nucleation and growth simulation of 5096 crystals with clustering induced by sinusoidal nucleation probability in each dimension. (b) Correlation functions measured on this simulation. The data fall above the 2-σ envelope at all scales but the smallest, reflecting the clustering of the simulation; the MCF data show no growth suppression, however.
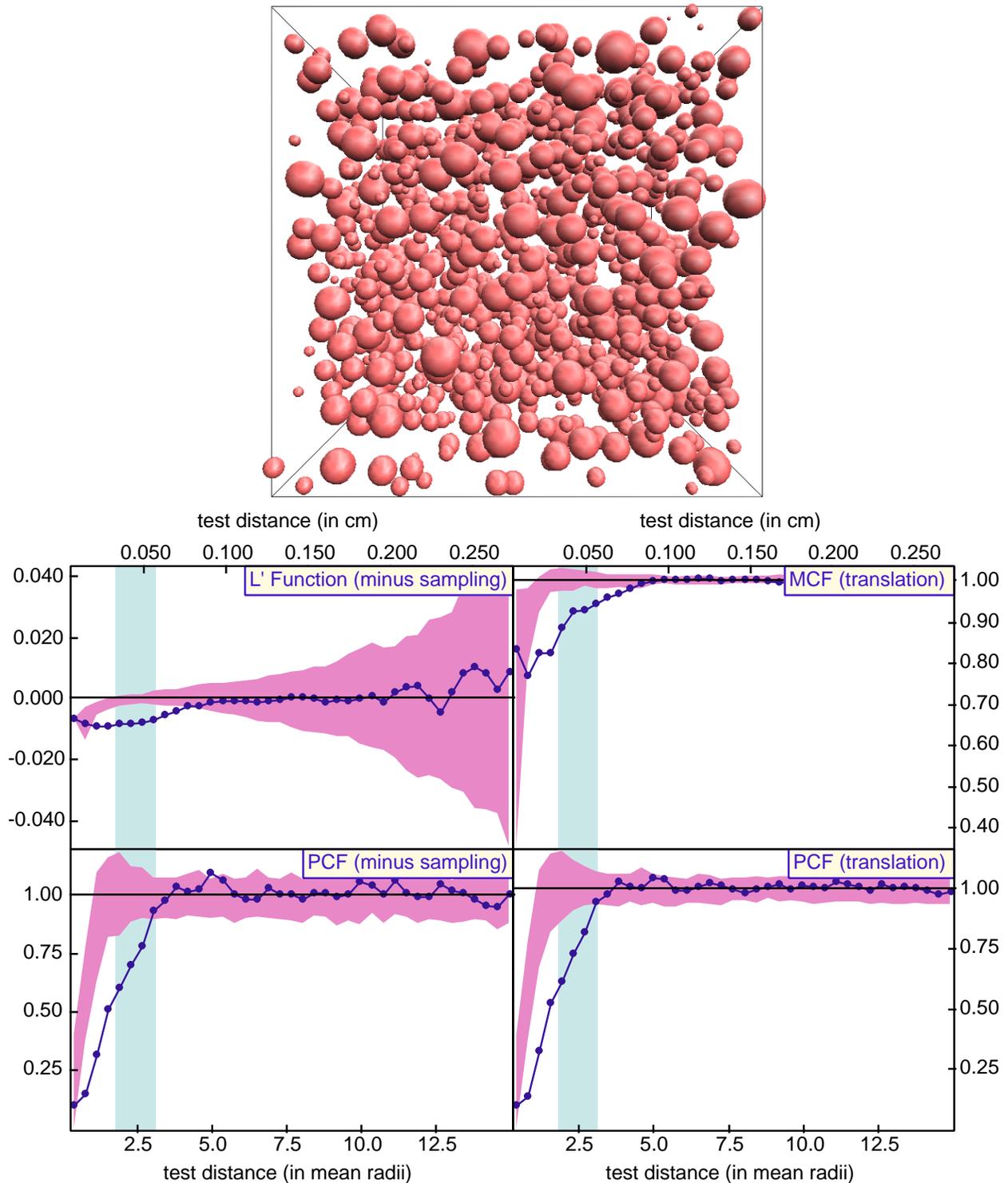
Figure 12. (a) Rendering of simulation DC-1, a thermally accelerated diffusion-controlled nucleation and growth simulation of 2971 crystals. (b) Correlation functions measured on this simulation. Data fall below the 2-σ envelope at scales up to the mean nearest-neighbor distance, as expected, and the MCF shows a correlation between separation and size, indicating growth suppression at small separations.
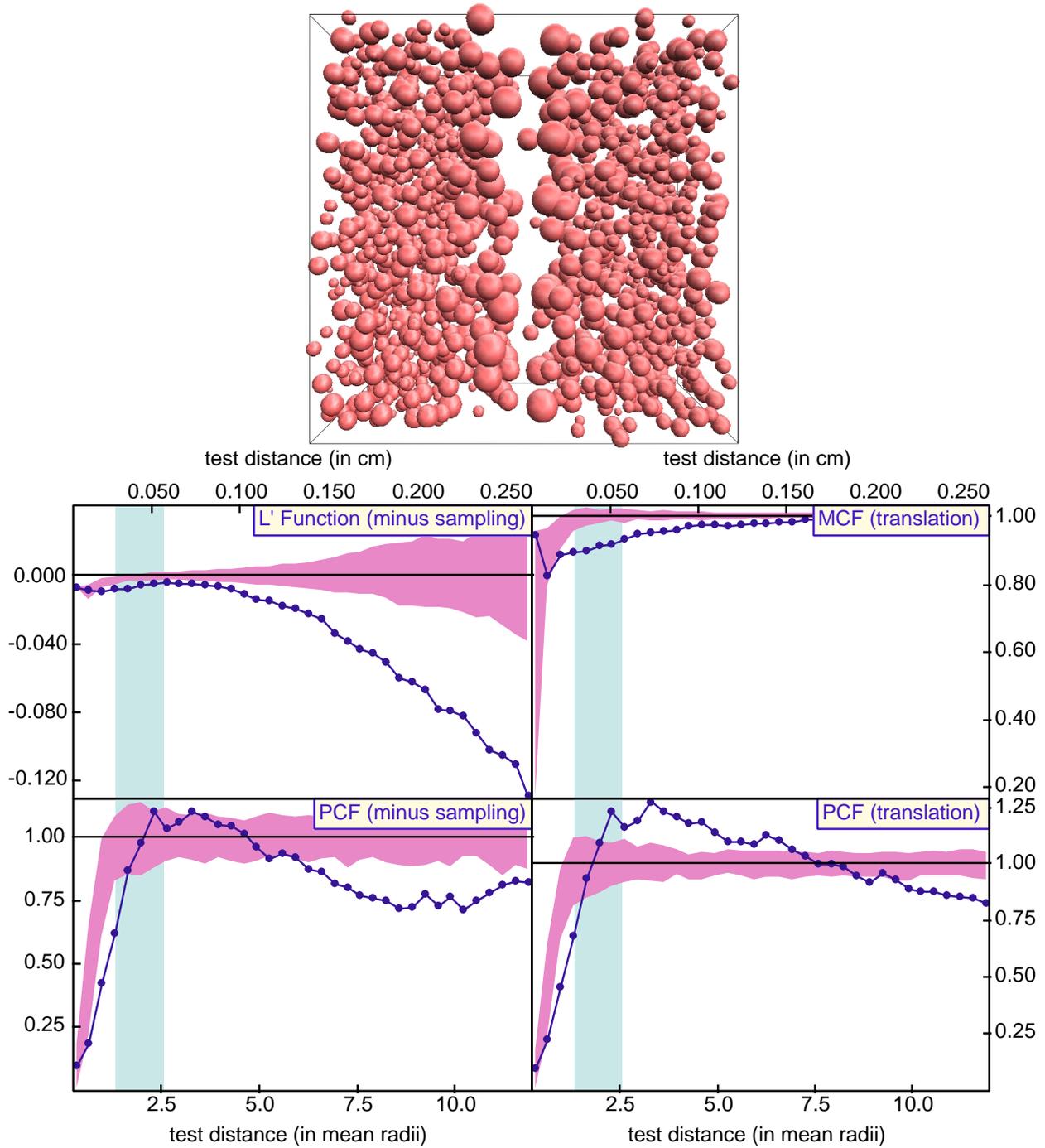
Figure 13. (a) Rendering of sub-volume of layered simulation DC-L4, in which layering is induced by a sinusoidal nucleation probability in one dimension imposed on a simulation of thermally accelerated diffusion-controlled nucleation and growth. (b) Correlation functions measured on this layered array of 1185 crystals. Envelope simulations incorporate nucleation probability distributions identical to DC-L4. Data fall below the 2-σ envelope at small scales, show clustering at larger scales, and then ordering at the scale of the layering, as expected. The MCF data are suspect because the simulation algorithm leads to large crystals bordering the sparse regions.
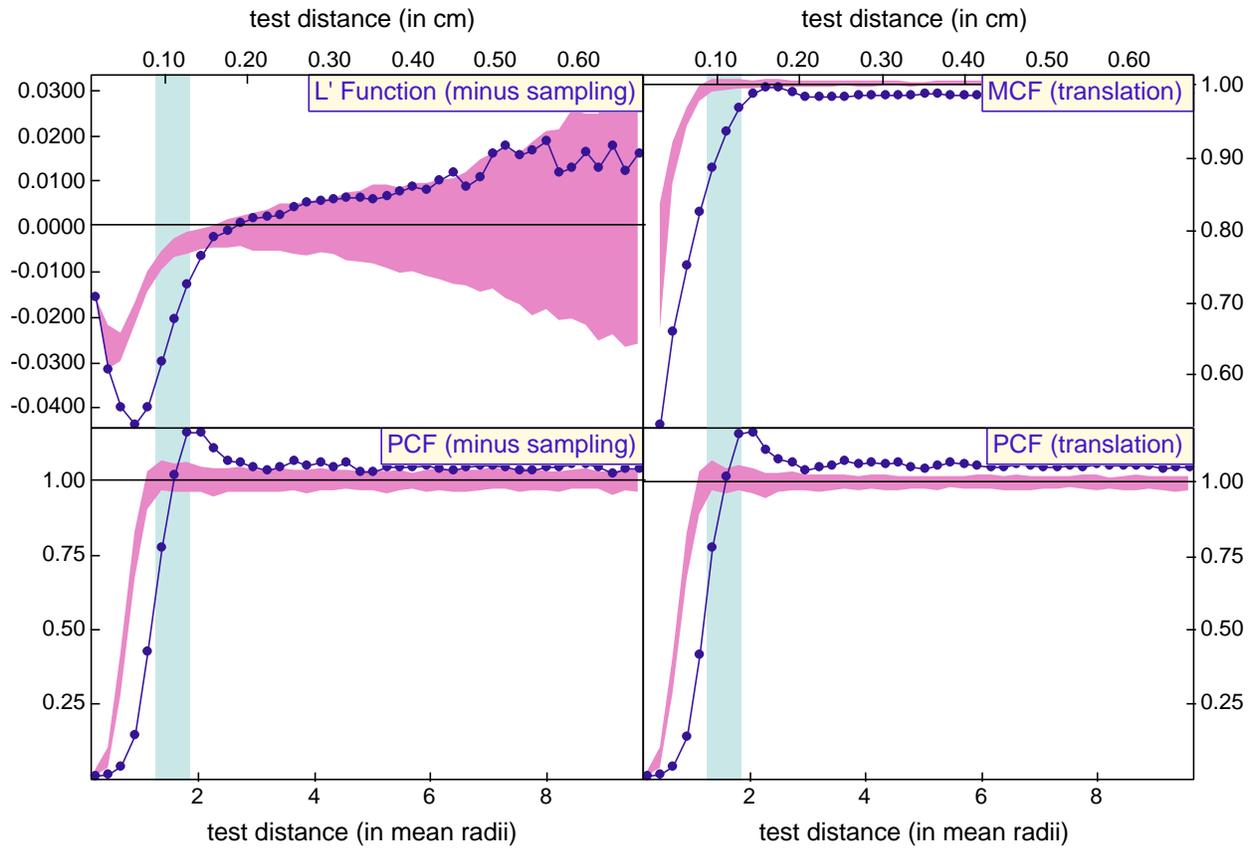
Figure 14. Correlation function data for sample PM1. The data show the result expected from the single-valued statistics: both ordering and growth suppression up to about the mean nearest-neighbor distance.
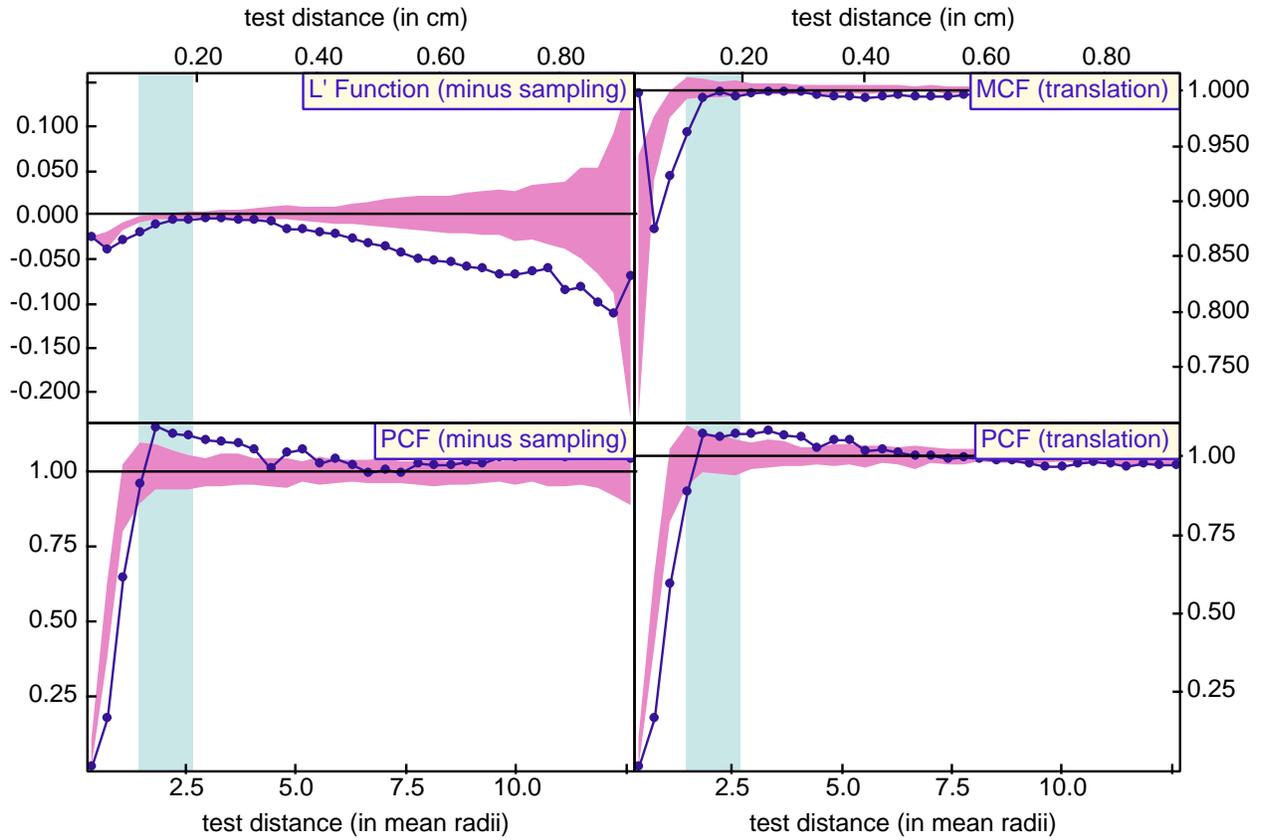
Figure 15. Correlation function data for sample PM2. The data show ordering of crystal centers and suppression of growth, in agreement with the single-valued statistics.
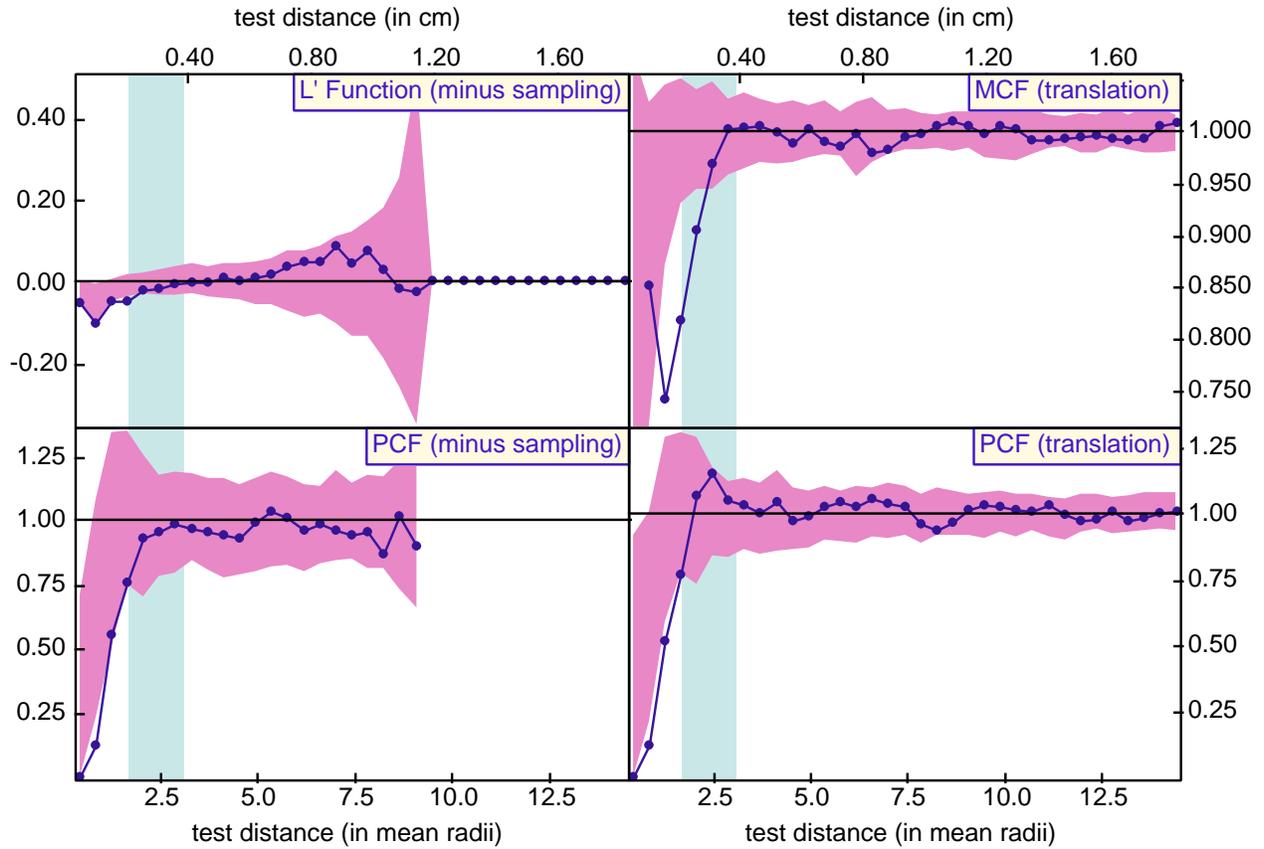
Figure 16. Correlation function data for sample MD. The data show slight negative excursions below the null-hypothesis region for the L' function and PCF, indicating barely significant ordering of crystal centers, and a strong excursion below the envelope for the MCF, indicating growth suppression for closely spaced crystals.
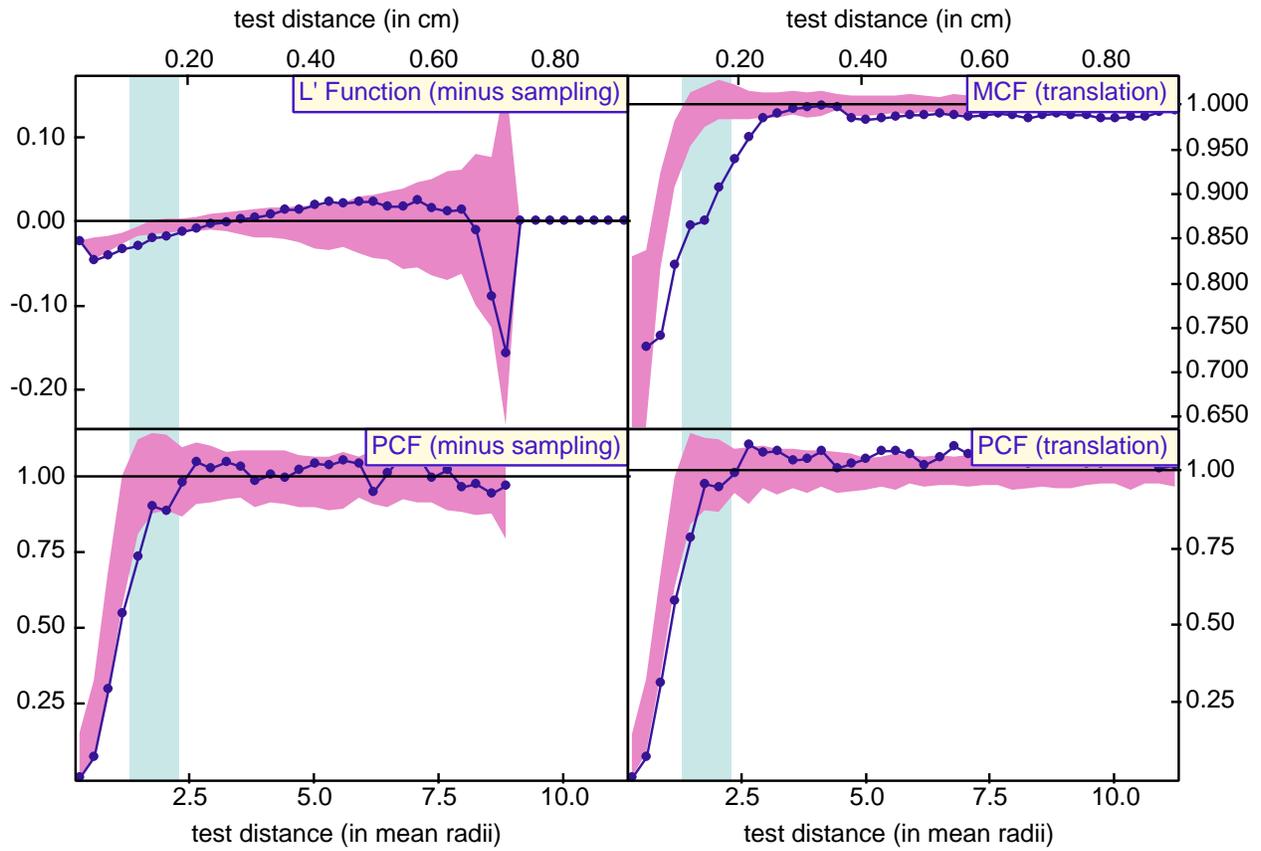
Figure 17. Correlation function data for sample WR1. The data show ordering of crystal centers and suppression of growth, in agreement with the single-valued statistics.
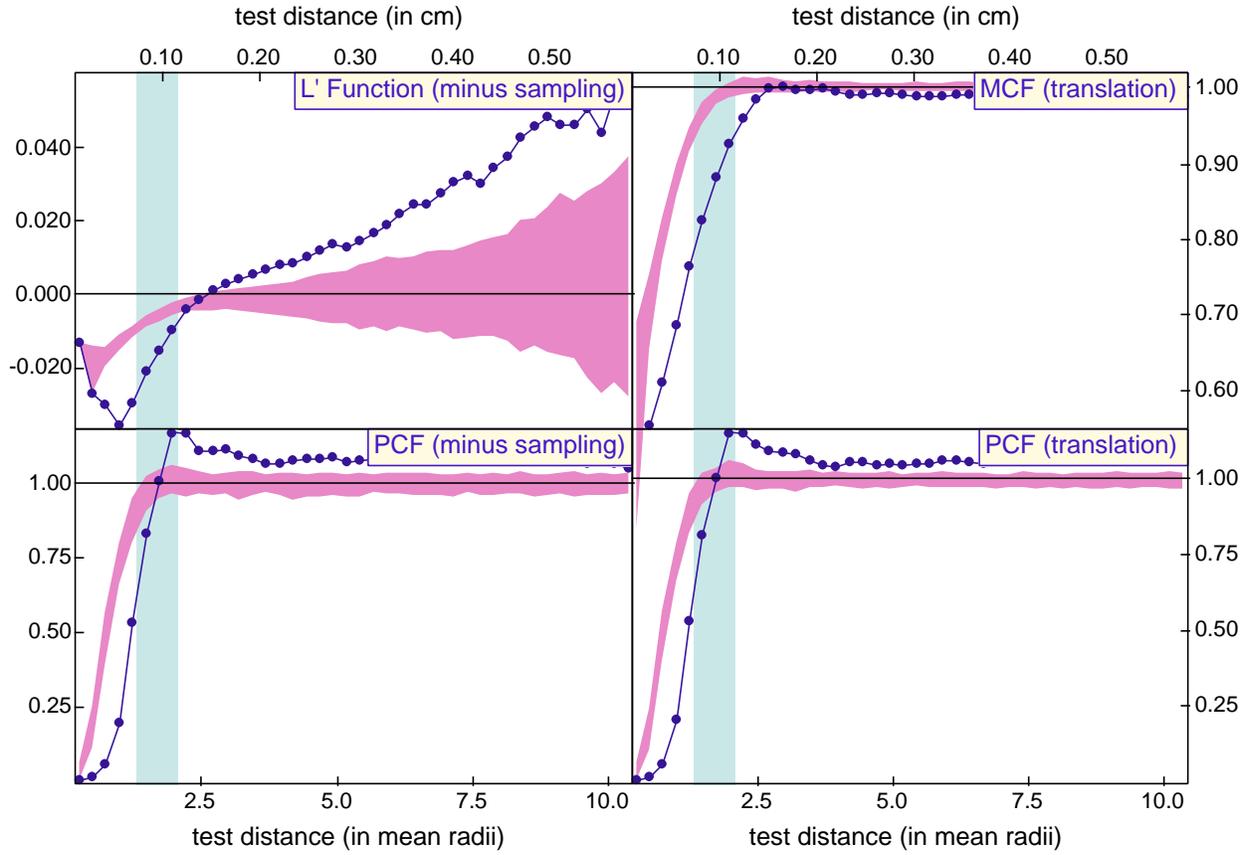
Figure 18. Correlation function data for sample WR2. The data show ordering of crystal centers and suppression of growth, in agreement with the single-valued statistics.
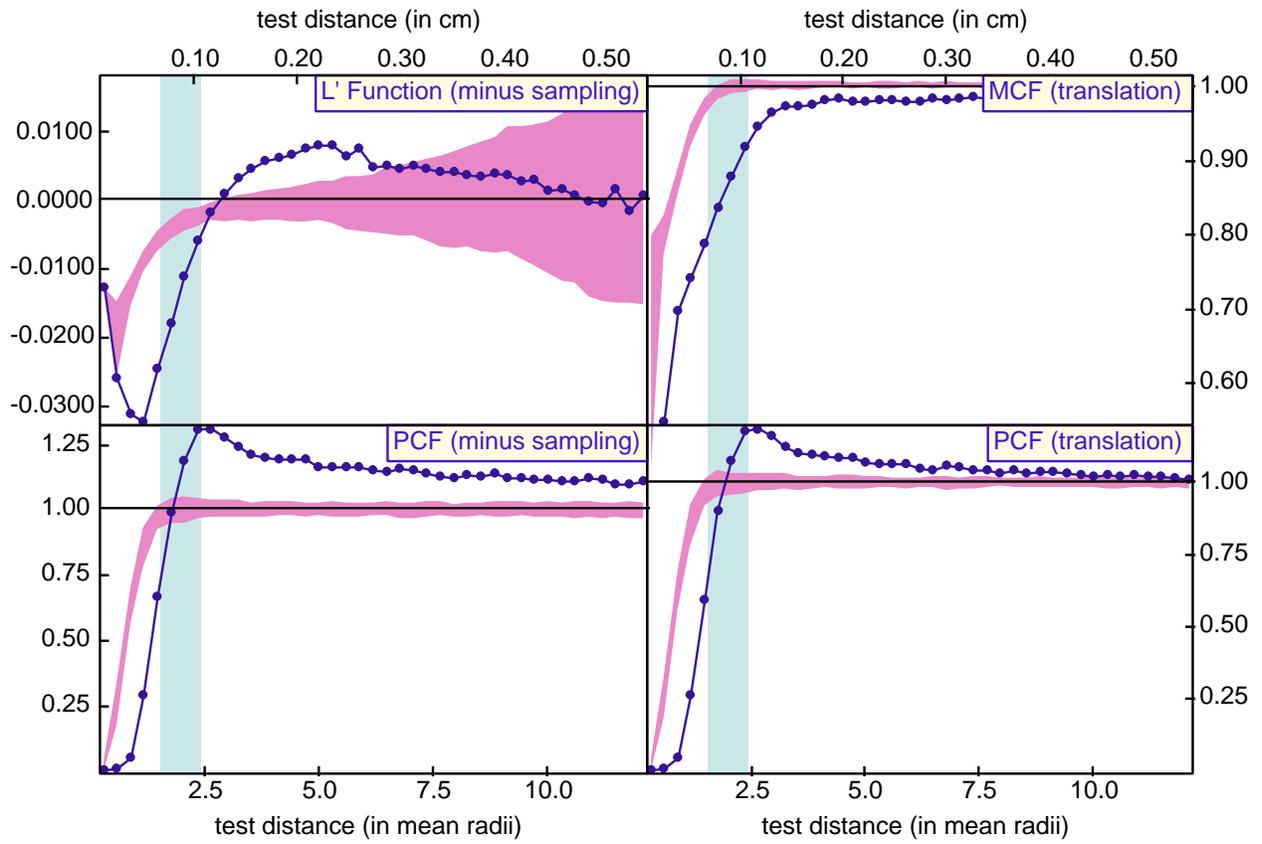
Figure 19. Correlation function data for sample WR3. The data show ordering of crystal centers and suppression of growth, in agreement with the single-valued statistics.
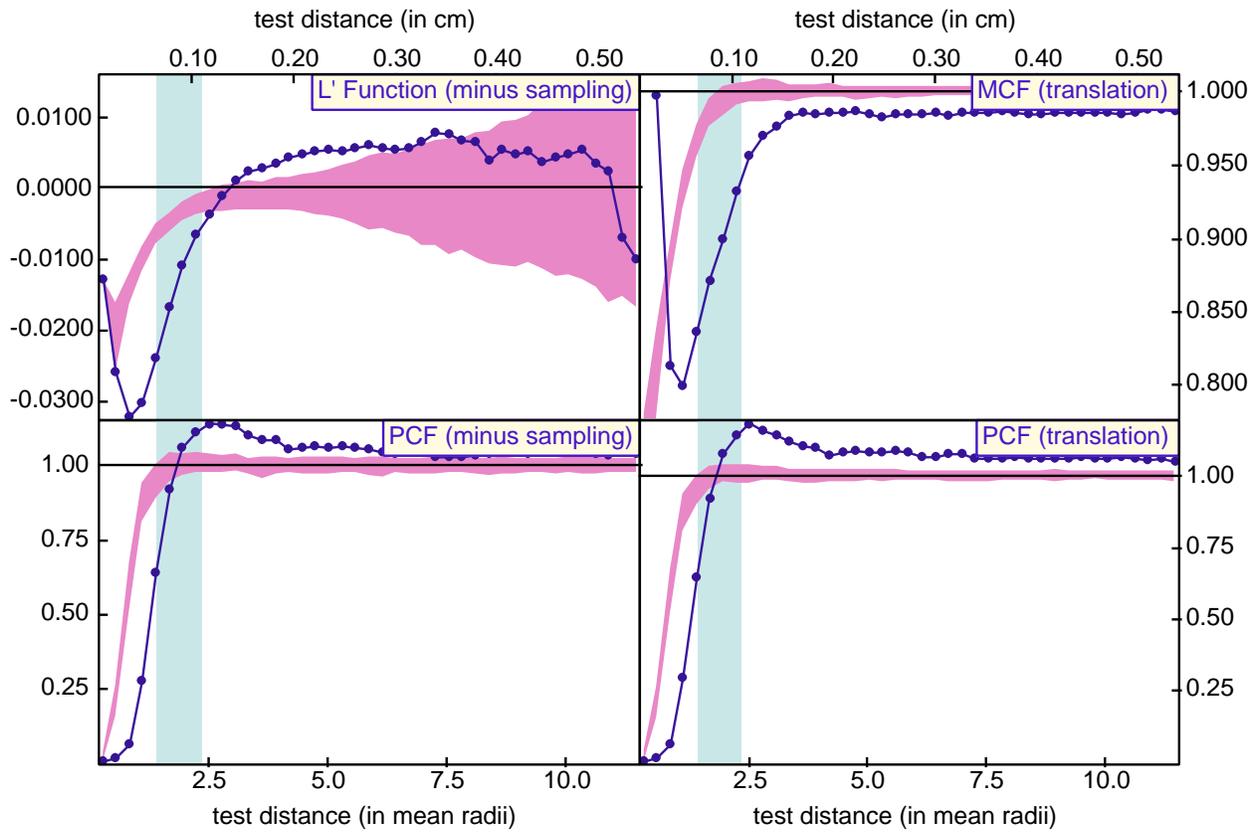
Figure 20. Correlation function data for sample WR4. The data show ordering of crystal centers and suppression of growth, in agreement with the single-valued statistics.